Exhibit A

Jerome M. Lewis

273 Upland Avenue
Newton, Massachusetts 02461
Telephone: 617-964-4055

Work Experience

Advanced Magnetics Inc., Pharmaceuticals
Cambridge, Massachusetts
Vice President - Scientific Operations, 1991 - Present
Director of Scientific Operations, 1989 - 1991
Director of Magnetic Resonance Imaging, 1987 - 1989
Senior Scientist, 1986 – 1987

The company has two approved drug products Feridex I. V.® and GastroMark® and several other drug products at various stages of development. I have been with the company since it started drug development.

Manufacturing Accomplishments at Advanced Magnetics Inc.

- Managed the production, production engineering, and facilities departments. Responsible for manufacturing, product development and scale-up.
- Responsible for the manufacturing and microbiological sections of NDAs and INDs, both US and foreign. Full knowledge of cGMPs. Company has received no deficiencies on FDA GMP and PAI inspections.
- Negotiated corporate contracts
- Consultant to Regulatory Department
- Implemented cost accounting system

Scientific Accomplishments at Advanced Magnetics Inc.

- Principal Investigator, National Cancer Institute
  Small Business Innovation Grants (Phase 1 (1986)
  and Phase 2 (1988-1990)
  "Ferrite Particles as NMR Imaging Contrast Agents"
  Phase 1 (1999) "Sentinel Lymph Node Staging with
  Magnetite Nanoparticles"
- Published scientific articles and received patents for both basic and developmental research which resulted in saleable products.
- Headed R&D group which developed GastroMark®
- Head of Chemistry R&D

Facilities Accomplishments at Advanced Magnetics Inc.

- Design, budget, and supervise construction of company's facilities including clean rooms, WFI systems, pollution control systems, GMP warehousing, bottling and labeling facilities, R&D and QC laboratories.

Petroferm Research Inc., Biotechnology & Specialty Chemicals
Cambridge, Massachusetts
Senior Scientist, 1981- 1986

Managed the Research Chemical Group, which developed surfactants and stabilizers for the petroleum industry. Responsible for all regulatory issues at the Massachusetts facility.
Solely responsible for the construction of the Massachusetts facility.

Clinical Assays (Division of Baxter Travenol)
An Immunodiagnostics Company
Cambridge, Massachusetts
Manager, Technical Support, 1980 - 1981
Senior Scientist, 1979 –1980

Managed the Technical Support Department, which was responsible for the maintenance and modernization of all company products including development of new antibodies and tracers for coated tube technology.

U.S. Army Environmental Hygiene Agency,Pollution Control
Edgewood, Maryland
Chemist, Military Service, 1971- 1973
Performed Environmental Surveys at Government and Industrial Sites.
Developed Analytical Methods

Education

Masters in Business Administration-Boston University, 1981 - 1983

Postdoctoral Fellow-Massachusetts Institute of Technology, 1977 - 1979

Ph.D. Bioorganic Chemistry-Boston University, 1973 - 1977

B.S. Chemistry-Michigan Technological University, 1967 - 1971

Representative Publications & Patents

"MR Imaging of Murine Artritis Using Ultrasmall Superparamagnetic Iron Oxide Particles", Dardzinski, B.J., Schmithorst, V.J., Holland, S.K., Bovin, G.P., Imagawa, T., Watanbe, S., Lewis, J.M., and Hirsch, R., Magnetic Resonance Imaging, 2001, 19, 1209-1216.

"Interstial MR Lymphangiography for the Detection of Sentinel Lymph Nodes", Torchia, M.G., Nason, R., Danzinger, R., Lewis, J.M., and Thliveris, J.A., J. of Surgical Oncology, 2001, 78, 151-157.

"Use of USPIO-Induced Magnetic Susceptibility Artifacts to Identify Sentinel Lymph Nodes and Lymphatic Drainage Patterns. I. Dependence of Artifact Size with Subcutaneous Combidex® Dose in Rats, Rogers, J.M., Jung, C.W., Lewis, J.M., and Groman, E.V., Magnetic Resonance Imaging, 1998, 8, pp. 917-923.

"Endotoxin-Free Polysaccharides", Lewis, J.M., U.S. Patent 5,589,591, 1996.

"Delivery of Therapeutic Agents to Receptors Using Polysaccharides", Enriquez, P., Groman, E., Josephson, L., Jung, C., Lewis, J.M., Menz, E., U.S. Patent 5,554,386, 1996

"Arabinogalactan Derivatives and Uses Thereof", Enriquez, P., Palmacci, S., Josephson, J., and Lewis, J.M., U.S. Patent 5,478,576, 1995

"Visualization of Superior Mesenteric Lymph Nodes by the Combined Oral and Intervenous Administration of the Ultrasmall Superparamagnetic Iron Oxide, AMI-227", Rogers, J., Lewis, J.M., and Josephson, L. Magnetic Resonance Imaging, 1995, 12, pp. 1161-1165.

"The Use of AMI-227 as an Oral Contrast Agent for Magnetic Resonance Imaging", Rogers, J., Lewis, J.M., and Josephson, L. Investigative Radiology 1994, 29, S81-S82.

"Use of AMI-227 as an Oral Contrast Agent", Rogers, J., Lewis, J., and Josephson, L., Magnetic Resonance Imaging, 1994, pp S31-39.

"Targeting of Therapeutic Agents Using Polysaccharides", Josephson, L, Groman, E.V., Jung, C, and Lewis, J.M., U.S. Patent 5,336,506, 1994.

"Vascular Magnetic Resonance Imaging Agent Comprising Nanoparticles", Menz, E.T., Kenny, F.E., Groman, E.V., Josephson, L, and Lewis, J.M., U.S. Patent 5,314,679, 1994.

"Hydrated Biodegradable Superparamagnetic Metal Oxides", Groman, E.V., Josephson, L., Lewis, J.M., U.S. Patent 5,219,554, 1993

"Hydrophobically Modified Proteins", Neataas, E., Hrebenar, K.R., Lewis, J.M., andWhitesides, G.M., U.S. Patent 5,212,235.

"Silanized Biodegradable Superparamagnetic Metal Oxides as Contrast Agents for Imaging the Gastrointestinal Tract", Groman, E.V., Josephson, L., Lewis, J.M., U.S. Patent 5,069,126, 1991.

"Vascular Magnetic Imaging Method and Agent Comprising Biodegradable Superparamagnetic Metal Oxides", Lewis, J. M., Menz, E.T., Kenny, F.E., Groman, E.V., Josephson, L., U. S. Patent 5,055,288, 1991.

"A Functionalized Superparamagnetic Iron Oxide Colloid as a Receptor Directed MR Contrast Agent", Josephson, L., Groman, E.V., Menz, E., Lewis, J.M., Bengle, H. Mag. Res. Imag. 1990, 8, 637-646.

"Biodegradable Superparamagnetic Metal Oxides as Contrast Agents for MR Imaging", Groman, E.V., Josephson, L., Lewis, J.M., U. S. Patent 4,951,675, 1990.

"First Clinical Trial of a New Superparamagnetic Iron Oxide for Use as an Oral Gastrointestinal Contrast Agent in MR Imaging", Hahn, P.F., Stark, D.D., Lewis, J.M., Saini, S., Elizondo, G., Weissleder, R., Fretz, C.J., Ferrucci, J.T. Radiology 1990, 175, 695-700.

"Biologically Degradable Superparamgnetic Materials For Use in Clinical Applications", Groman, E.V., Josephson, L., Lewis, J.M., U. S. Patent 4,827,945, 1989.

"Superparamagnetic Iron Oxide: Pharmacokinetics and Toxicity", Weissleder, R., Stark, D.D., Engelstad, B.L., Bacon, B.R., Compton, C.C., White, D.L., Jacobs, P., Lewis, J.M. AJR 1989, 152, 167-173.

"The Effects of Iron Oxides on Proton Relaxivity", Josephson, L., Lewis, J.M., Jacobs, P., Hahn, P.F., Stark, D.D. Mag. Res. Imag. 1988, 6, 647-653.

"Ferrite Particles for Bowel Contrast in MR Imaging: Design Issues and Feasibility Studies", Hahn, P.F., Stark, D.D., Saini, S., Lewis, J.M., Wittenberg, J., Ferrucci, J.T. Radiology 1987, 164, 37-41.

"Hypothyroid Control Serum", Lewis, J.M., Parsons, H., U. S. Patent 4,431,741, 1984.

"Practical Synthesis of 5-Phospho-D-a-1-Pyrophosphate (PRPP): Enzymatic Routes from Ribose-5-Phospate or Ribose", Gross, A., Abril, O., Lewis, J.M. J. Am. Chem. Soc. 1983, 105, 7428-7435.

"Cross Reactivity in Theophylline RIA Kit Decreased", Lewis, J.M. Clinical Chem. 1981, 27, 1316.

"Conversion of Adenosine Moieties for RNA into ATP for Use in Cofactor Recycling", Leuchs, H.J., Lewis, J.M., Rois-Mercadillo, V.M., Whitesides, G.M. J. Am. Chem. Soc. 1979, 101, 5829.

"An Improved Synthesis of Diammonium Acetyl Phosphate", Lewis, J.M., Haynie, S.L., Whitesides, G.M. J. Org. Chem. 1979, 44 , 8664-865.

"Amidophosphoribosyltransferase (Chicken Liver)", Lewis, J. M., Hartman, S. H. Methods Enzymol., 1978, 51, 171-178.

Risk-Based CMC Microbiology Review

- Sterile Products
- Non-Sterile Products

Exhibit B

Sterile Products- 1

- Risk in making changes to sterile products relates to the process - not the product.
  - Terminal sterilization processes present a lower risk than aseptic processes.
  - Aseptic processes present greater technical challenges and risk

Sterile Products- 2

- Certain changes to processing of "low risk products" will still require a supplement
  - Major changes in sterilization technology (e.g., filtration to gamma irradiation)
  - Deleting a step in a sterilization process
  - Changing critical parameters or specifications in the sterilization process

Sterile Products- 3

- Many changes do not negatively affect sterility assurance -> annual reportable
  - Minor changes to container/closure
  - Equipment used prior to the sterilization step
  - Terminal sterilization autoclave loading patterns
  - Lyophilization cycle

Non-Sterile Products

- No microbiological concerns for oral dosage forms, transdermals, suppositories, and inherently anti-microbial products
- Certain non-aqueous products (MDIs, nasal sprays, dry-powder inhalers) were considered "low risk"

Manufacturing Process-Associated Changes

- Requests for Guidance Documents and Definitions
  - Categories to file changes
  - More examples and definitions
- Inconsistent review findings and recommendations (inter-office, inter-center, field)

Sterile Products- 1

- Risk in making changes to sterile products relates to the process - not the product.
  - Terminal sterilization processes present a lower risk than aseptic processes.
  - Aseptic processes present greater technical challenges and risk

The rules governing medicinal products in the European Union

Exhibit C

Volume 4

Good manufacturing practices

Medicinal products for human and veterinary use

1998 Edition

EUROPEAN COMMISSION
Directorate General III – Industry
Pharmaceuticals and cosmetics

Exhibit 1

EUROPEAN PHARMACOPOEIA

3rd Edition

5.1.1. METHODS OF PREPARATION OF STERILE PRODUCTS

Sterility is the absence of viable micro-organisms. The sterility of a product cannot be guaranteed by testing; it has to be assured by the application of a suitably validated production process. It is essential that the effect of the chosen sterilisation procedure on the product (including its final container or package) is investigated to ensure effectiveness and the integrity of the product and that the procedure is validated before being applied in practice. It is recommended that the choice of the container is such as to allow the optimum sterilisation to be applied. Failure to follow meticulously a validated process involves the risk of a non-sterile product or of a deteriorated product. Revalidation is carried out whenever major changes in the sterilisation procedure, including changes in the load, take place. It is expected that the principles of good manufacturing practice (as described in, for example, the European Community Guide to GMP) will have been observed in the design of the process including, in particular, the use of:

- qualified personnel with appropriate training,
- adequate premises,
- suitable production equipment, designed for easy cleaning and sterilisation,
- adequate precautions to minimise the bioburden prior to sterilisation,
- validated procedures for all critical production steps,
- environmental monitoring and in-process testing procedures.

The precautions necessary to minimise the pre-sterilisation bioburden include the use of components with an acceptable low degree of microbial contamination. Microbiological monitoring and setting of suitable action limits may be advisable for ingredients which are liable to be contaminated because of their origin, nature or method of preparation.

The methods described here apply mainly to the inactivation or removal of bacteria, yeasts and moulds. For biological products of animal or human origin or in cases where such material has been used in the production process, it is necessary during validation to demonstrate that the process is capable of the removal or inactivation of relevant viral contamination. Guidance on this aspect is provided in, for example, the appropriate European Community Notes for Guidance.

Wherever possible, a process in which the product is sterilised in its final container (terminal sterilisation) is chosen. When a fully validated terminal sterilisation method by steam, dry heat or ionising radiation is used, parametric release, that is the release of a batch of sterilised items based on process data rather than on the basis of submitting a sample of the items to sterility testing, may be carried out, subject to the approval of the competent authority.

If terminal sterilisation is not possible, ... bacteria-retentative filter or aseptic processing is used; wherever possible, appropriate additional treatment of the product (for example, heating of the product) in its final container is applied. In all cases, the container and closure are required to maintain the sterility of the product throughout its shelf-life.

Sterility Assurance Level (SAL)

Where appropriate reference is made within the methods described below, to a 'sterility assurance level' or 'SAL'. The achievement of sterility within any one item in a population of items submitted to a sterilisation process cannot be guaranteed nor can it be demonstrated. The inactivation of micro-organisms by physical or chemical means follows an exponential law; thus there is always a finite statistical probability that a micro-organism may survive the sterilising process. For a given process, the probability of survival is determined by the number, types and resistance of the micro-organisms present and by the environment in which the organisms exist during treatment. The SAL of a sterilising process is the degree of assurance with which the process in question renders a population of items sterile. The SAL for a given process is expressed as the probability of a non-sterile item in that population. An SAL of 10^{-6}, for example, denotes a probability of not more than one viable micro-organism in 1×10^6 sterilised items of the final product. The SAL of a process for a given product is established by appropriate validation studies.

METHODS AND CONDITIONS OF STERILISATION

Sterilisation may be carried out by one of the methods described below. Modifications to, or combinations of, these methods may be used provided that the chosen procedure is validated both with respect to its effectiveness and the integrity of the product including its container or package.

For all methods of sterilisation the critical conditions of the operation are monitored in order to confirm that the previously determined required conditions are achieved throughout the batch during the whole sterilisation process This applies in all cases including those where the reference conditions are used.

Terminal Sterilisation

For terminal sterilisation it is essential to take into account the non-uniformity of the physical and, where relevant, chemical conditions within the sterilising chamber. The location within the sterilising chamber that is least accessible to the sterilising agent is determined for each loading configuration of each type and size of container or package (for example, the coolest location in an autoclave). The minimum lethality delivered by the sterilising cycle and the reproducibility of the cycle are also determined in order to ensure that all loads will consistently receive the specified treatment.

Having established a terminal sterilisation process, knowledge of its performance in routine use is gained wherever possible, by monitoring and suitably recording the physical and, where relevant, chemical conditions achieved within the load in the chamber throughout each sterilising cycle.

Feridex I.V.®
(ferumoxides injectable solution)

BERLEX

Exhibit E

REV 06

DESCRIPTION

Feridex I.V.® (ferumoxides injectable solution) is a sterile aqueous colloid of superparamagnetic iron oxide associated with dextran for intravenous (i.v.) administration as a magnetic resonance imaging contrast media. Chemically, ferumoxides is a non-stoichiometric magnetite, of average formula $FeO_{1.44}$. Each milliliter of Feridex I.V. contains 11.2 milligrams of iron and 61.3 milligrams of mannitol at a pH of 5 to 9. The formulation also contains dextran (5.6 - 9.1 mg/mL) and citrate (0.25 - 0.53 mg/mL). The osmolality is approximately 340 mOsm/kg; specific gravity is 1.04. Feridex I.V. is a black to reddish-brown aqueous colloid.

CLINICAL PHARMACOLOGY

General: Feridex I.V. is an intravenously injected colloidal superparamagnetic iron oxide associated with dextran. It is a magnetic resonance imaging (MRI) contrast agent and is taken up by cells of the reticuloendothelial system (RES).

Pharmacokinetics:

Three healthy, adult male volunteers received a dose of Feridex I.V. 0.56 mg of Fe/kg (diluted in 100 mL of 5% dextrose and intravenously infused over 30 minutes). In these subjects, the mean ± SD peak serum iron concentration was 5.5 ± 0.6 µg/mL, elimination half-life was 2.4 ± 0.2 hours and total clearance 28.5 ± 1.6 mL/min. Feridex I.V. was completely cleared from the blood by 25 hours after administration. Less than 2% of the drug was excreted in the urine, as expected for iron.

At 24 hours, serum iron increased and the percent saturation of iron binding capacity decreased in a dose-dependent fashion. By 7 days, serum iron returned to pre-administration levels, and serum ferritin increased. These results are consistent with the iron in Feridex I.V. entering the usual iron metabolism cycle. Animal pharmacokinetics studies were consistent with these results in humans.

Imaging studies in rats showed a large decrease in liver signal intensity for the first 24 hours after dosing, followed by a gradual return to normal over 7 days. Radiotracer studies in rats were consistent with the iron in Feridex I.V. becoming part of the body iron pool. Histological studies in rats showed that the iron was in the RES and that it disappeared from the RES over 7 to 14 days with all evidence of iron gone by 14-28 days.

In human clinical studies, there was no difference in loss of signal intensity on images obtained between 0 - 3.5 hours after infusion. Loss of signal intensity decreased at 1 and 2 days.

Metabolism: The iron in Feridex I.V. enters the normal body iron metabolism cycle as evidenced by transient increases in serum iron values one day after administration and increase in serum ferritin values 7 days after administration. The amount of iron contained in a single dose is 39 mg for a 70 kg individual. This is less than 1/5 the amount of iron contained in one unit of whole blood.

Special Populations:

Geriatric/Pediatric: Pharmacokinetics in these populations were not studied. Patients enrolled in clinical trials were between 11 and 89 years old.

Gender: Women showed a higher pre-contrast signal intensity and hence a larger decrease in liver signal intensity in images. This is consistent with a lower baseline iron in women.

Race: Differences due to race were not noted.

Renal Insufficiency: Feridex I.V. is not renally cleared; no studies were performed in patients with renal insufficiency.

Hepatic Insufficiency: Patients with cirrhosis had less of a decrease in liver signal intensity than other patients with known or suspected liver lesions. Patients with cirrhosis also had a higher incidence of back pain. **(See ADVERSE REACTIONS section.)**

Hemochromatosis: Individuals with iron overload were not studied. Feridex I.V. contains iron. Literature reports suggested that Feridex I.V. will not add information to their MRI evaluations, since iron overload causes loss in liver signal intensity.

Drug-Drug Interactions: In rats, the simultaneous administration of heparin was found to prolong the half-life of Feridex I.V. in the blood. The effects of Feridex I.V. administration on heparin anticoagulation are not known.

Pharmacodynamics: Feridex I.V. shortens the relaxation times for nearby hydrogen atoms and reduces signal intensity in normal tissues. This results in signal loss (image darkening) on mid T1/T2 or strongly T2-weighted images. Tissues with decreased RES function (e.g., metastases, primary liver cancer, cysts and various benign tumors, adenomas, and hyperplasia) retain their native signal intensity, so the contrast between normal and abnormal tissue is increased.

CLINICAL TRIALS

Two clinical studies evaluated a total of 211 patients,(107 men and 104 women, 22-83 years of age) with a variety of known or suspected liver lesions. Of these patients, efficacy evaluations were completed on 96 patients in Study A, and 112 patients in Study B. At baseline, patients had a CECT (contrast enhanced computerized tomography) scan with any iodinated contrast agent and a non-contrast MRI (magnetic resonance imaging) within 24 hours before Feridex I.V. administration. Feridex I.V. (0.56 mg/kg) was administered intravenously over 30 minutes. Images were acquired up to 3.5 hours after the end of the infusion. The CECT, unenhanced MRI, and Feridex I.V. enhanced MRI images were read blindly (i.e., by radiologists who were not told of the patient's medical history or the presence of image contrast enhancing drugs). Results from blindly read images were compared to the final clinical diagnosis. The final clinical diagnoses were confirmed with histopathologic, surgical, or biopsy findings in 86 (41%) of patients. MRI scans were evaluated for the quantitative analysis of signal intensity in liver lesion(s), and by blinded evaluations of the resulting images for changes in number and location of lesions, delineation of lesion margins, presence or absence of lesions, and characterization of lesions.

Based upon these two studies, Feridex I.V. reduced the signal intensity of normal liver on T2 weighted pulse sequences to improve MRI contrast. Contrast to noise ratios were increased on T2 images and decreased on T1 images. Image interpretations for contrast enhancement, the number of lesions identified, and the sensitivity and specificity of the determination of whether an abnormal lesion was present are shown in the following table. The mean number of lesions seen before and after Feridex I.V. were comparable. The majority of new lesions (86%) were 0.5 cm-1.0 cm in size, but other lesions were seen that were <0.5 cm or >1.0 cm.

IMAGE INTERPRETATION RESULTS AFTER UNENHANCED MRI, CECT AND FERIDEX I.V. ENHANCED MRI IN TWO CLINICAL STUDIES OF PATIENTS WITH KNOWN OR SUSPECTED LIVER LESIONS**

Outcome Measure	Control Comparisons	Study A (N = 96)	Study B (N=112)
Contrast between normal and abnormal liver tissue seen on MRI	MRI Contrast Better with Feridex I.V. MRI Contrast Same with Feridex I.V. MRI Contrast Worse with Feridex I.V.	84% 13% 3% (p<0.01)	86% 12% 2% (p<0.01)
Number of Patients with Lesions Seen on MRI	Patients with: More before Feridex I.V. Same before and after Feridex I.V. More After Feridex I.V	 13% 62% 25%	 21% 51% 28%
Number of liver lesions seen on MRI (Mean ± SD)	MRI before Feridex I.V. after Feridex I.V.	7.3 ± 15.9 6.7 ± 10.4 (p=n.s.)	6.7 ± 14.8 7.3 ± 15.5 (p=n.s.)
Sensitivity/specificity for the	MRI before Feridex I.V. vs. Final diagnosis:*		

Copy

Specificity	71%	77%
MRI after Feridex I.V. vs. Final diagnosis:* Sensitivity Specificity	 95% 76%	 92% 85%
CECT vs. Final diagnosis:* Sensitivity Specificity	 96% 67%	 98% 58%

* Final diagnosis: e.g., by biopsy, surgical resection, autopsy, MRI procedures other than with Feridex I.V., CECT, ultrasound, or other clinical information.

** MRI (magnetic resonance image), CECT (contrast enhanced computerized tomography)

In various types of liver lesions, Feridex I.V. caused a smaller decrease in the signal intensity (59%-105% of the unenhanced) than in the surrounding liver (28%-41% of the unenhanced). The signal intensity changes are not characterized sufficiently to support distinguishing between types of lesions or diseases. Whether patients with cirrhosis have similar changes in signal intensity is not known.

PERCENT DECREASE IN MRI SIGNAL INTENSITY (SI) ON T2 IMAGES AFTER FERIDEX I.V.

Disease State	Surrounding Liver		Lesion in Question	
	N	% decrease in SI after Feridex I.V.	N	% decrease in SI after Feridex I.V.
Patients with benign, malignant, hepatocellular and non-hepatocellular lesions (excluding cirrhosis)	162	59-72%	153	0-41%

Imaging of the spleen by Feridex I.V. has not been adequately studied.

INDICATION AND USAGE

Feridex I.V. is indicated for I.V. administration as an adjunct to MRI (in adult patients) to enhance the T2 weighted images used in the detection and evaluation of lesions of the liver that are associated with an alteration in the RES.

CONTRAINDICATIONS

Feridex I.V. is contraindicated in patients with known allergic or hypersensitivity reactions to parenteral iron, parenteral dextran, parenteral iron-dextran, or parenteral iron-polysaccharide preparations.

WARNINGS

Anaphylactic-like reactions and hypotension have been noted in some patients receiving Feridex I.V., other iron and dextran containing formulations, or radiographic contrast media. In clinical trials, anaphylactic and allergic adverse events occurred in 11/2240 (0.5%) of the patients who received Feridex I.V. These events include dyspnea, other respiratory symptoms, angioedema, generalized urticaria, and hypotension; and required treatment.

Acute severe back, leg or groin pain occurred in some patients. In clinical trials, 55/2240 (2.5%) of the patients experienced pain that was severe enough to cause interruption or discontinuation of the infusion. In most patients, the symptoms developed within 1 to 15 minutes (up to 45 minutes). Some patients required treatment with corticosteroids, intravenous fluids or muscle relaxants. Pain may occur alone or with other symptoms such as hypotension and dyspnea. Patients with both pain and allergic symptoms received treatment with a combination of medications directed toward each event. **(See ADVERSE REACTIONS section.)**

Patients with autoimmune disease have not been studied with Feridex I.V., but have been reported in published literature to have a high rate of adverse reactions to injectable iron formulations.

If hypersensitivity, or moderate to severe pain occurs, the injection should be stopped, and symptomatic treatment should be given.

A fully equipped emergency cart, or equivalent supplies and equipment, and personnel competent in recognizing and treating anaphylactic or anaphylactoid reactions should be available.

PRECAUTIONS

GENERAL: THE DECISION TO USE CONTRAST ENHANCEMENT SHOULD INCLUDE A CONSIDERATION OF THE RISK OF THE DRUG, THE RISK OF THE PROCEDURE, THE EXPECTED BENEFIT OF THE IMAGE AND THE PATIENT'S UNDERLYING DISORDER. THE DECISION TO USE FERIDEX I.V. SHOULD BE BASED UPON CAREFUL EVALUATION OF CLINICAL DATA, OTHER RADIOLOGIC DATA, AND THE RESULTS OF UNENHANCED MRI.

Patients receiving contrast agents and especially those who are medically unstable must be closely supervised. Diagnostic procedures which involve the use of any contrast agent should be carried out under the direction of personnel with the prerequisite training and with a thorough knowledge of the particular procedure to be performed.

After parenteral administration of a contrast agent, competent personnel, a fully equipped emergency cart or equivalent, and emergency facilities should be available for at least 60 to 120 minutes.

Immunologic Reactions:

The possibility of a reaction including serious, life-threatening, fatal, anaphylactoid or cardiovascular reactions should always be considered. Increased risk is associated with a known sensitivity to iron or dextran, history of previous reaction to a radiographic contrast agent, known allergies, other hypersensitivities, and underlying immune disorders, autoimmunity or immunodeficiencies that predispose to specific or non specific mediator release.

Skin testing cannot be relied upon to predict severe reactions and skin testing may itself be hazardous to the patient. A thorough medical history with emphasis on allergy and hypersensitivity, immune, autoimmune and immunodeficiency disorders, and prior receipt of and response to the injection of any contrast agent, may be more accurate than pretesting in predicting potential adverse reactions.

Feridex I.V., which contains iron, should be used with caution in patients with disorders associated with iron over load (e.g., hemosiderosis, chronic hemolytic anemia with frequent blood transfusions).

Extreme caution during injection of a contrast agent is necessary to avoid extravasation. This is especially important in patients with severe arterial or venous disease.

Repeat Procedures: If the physician determines that imaging needs to be repeated, based on the pharmacodynamics of Feridex I.V., repeat images could be obtained up to 3.5 hours after the original infusion without re-injection. Data on timing for and safety of repeated injections are not available. **(See CLINICAL PHARMACOLOGY section.)**

Copy

ADVERSE EVENTS IN ≥ 0.5% OF THE 1535 PATIENTS IN CONTROLLED CLINICAL TRIALS WITH FERIDEX I.V.

Categories	Adverse Event	Number of Patients (%)
Number of patients who received Feridex I.V.		1535
Number of patients with any adverse event		144 (9.4%)
Digestive System	Nausea	11 (0.7%)
Body as a whole	Total (pain all sources) Pain Back/Leg/Pain Leg Headache Pain Chest	65 (4.2%) 56 (3.6%) 13 (0.8%) 10 (0.7%)
Hypersensitivity	Total (hypersensitivity all sources) Vasodilation Urticaria/Erythematous Rash/Rash Dyspnea	53 (3.4%) 33 (2.1%) 12 (0.7%) 8 (0.5%)

The following adverse reactions were observed in <0.5% of the subjects receiving Feridex I.V.: DIGESTIVE: diarrhea, vomiting, anorexia; BODY PAIN: pain abdomen, pain neck, fatigue, fever; CARDIOVASCULAR: hypertension, hypotension, arrhythmias; NERVOUS: dizziness, paresthesia; SKIN AND APPENDAGES: pruritus, sweating; SPECIAL SENSES: abnormal vision, taste perversion; RESPIRATORY: cough, epistaxis, rhinitis.

(See sections on CONTRAINDICATIONS, WARNINGS and PRECAUTIONS.)

In 705 patients who received Feridex I.V. in other trials, similar adverse events were reported.

OVERDOSE

Overdose with Feridex I.V. has not been reported. Acute toxicity is apt to be related to iron overload, acute back pain and allergic events. Chronic administration of therapeutic iron dextran in excess of the total amount of iron needed for iron stores may lead to hemosiderosis.

A study of (59Fe) complexed iron-dextran utilizing isotonic saline in a 4-hour in vitro dialysis run indicated that less than 0.5% of the injected radio labeled iron dextran traversed the dialysis membrane. Feridex I.V. contains iron associated with dextran. Whether Feridex I.V. is dialyzable is not known.

DOSAGE AND ADMINISTRATION

Dose

The recommended dosage of Feridex I.V. is 0.56 milligrams of iron (0.05 mL Feridex I.V.) per kilogram of body weight, that is diluted in 100 mL of 5% dextrose solution and given over 30 minutes. (See Drug Preparation Section). The diluted drug is administered through a 5 micron filter at a rate of 2 to 4 milliliters per minute.

Feridex I.V. should not be administered undiluted.

Drug Preparation

1. The vial should be used at room temperature. Mix by inverting the vial 10 to 20 times.
2. Draw up the appropriate dose of Feridex I.V. into a sterile syringe.
3. Dilute Feridex I.V. by injecting it into 100 mL of 5% dextrose solution (D5W).
4. The bag should be inverted two or three times to assure dilution.
5. The drug product should be administered within 8 hours following dilution.

Imaging

Post-contrast imaging may begin immediately after the dose is infused and may be performed up to 3.5 hours after the end of the infusion. T2-weighted pulse sequences provide the maximum contrast effect.

HOW SUPPLIED

Feridex I.V. is black to reddish brown liquid containing 11.2 mg Fe/mL (56 mg of iron/vial) in a vial with a tear off seal. Feridex I.V. is supplied in 5 mL single dose vials in boxes of 5 (NDC59338-7035-5) and 10 (NDC 59338-7035-0). An administration filter is supplied for each vial.

Feridex I.V. is stable for 24 hours after dilution.

STORAGE

Storage at 2-30 °C (35-86 °F). DO NOT FREEZE.
If there are indications that the package has been exposed to freezing, DO NOT USE.

Rx Only

The following patents have claims directed to the drug: U.S.P. 4,770,183, U.S.P. 4,827,945, U.S.P. 4,951,675, U.S.P. 5,055,288, U.S.P. 5,102,652, U.S.P. 5,219,554, U.S.P. 5,248,492

Mfd. for Berlex Laboratories, Wayne, NJ 07470

Mfd. by Advanced Magnetics, Inc., Cambridge, MA 02138

Revised March 1998 Printed in USA 6102 REV 06

Information for Patients

Patients receiving Feridex I.V. should be instructed to inform their physician or health care provider:

1. If you are pregnant or nursing. **(See PRECAUTIONS - PREGNANCY - Teratogenic Effects - Pregnancy Category C section.)**

2. If you are allergic to iron or dextran containing drugs or if you had any reactions to previous injections of dyes used for x-ray procedures. Also, inform your physician or health care provider if you are allergic to any other drugs or food, or if you have immune, autoimmune or immune deficiency disorders. **(See PRECAUTIONS - GENERAL section.)**

3. About all medications you are currently taking, including non-prescription (over-the-counter) drugs and vitamins, before you have this procedure.

Patients should be informed that:

1. Feridex I.V. has been prescribed for liver enhancement during MRI.

2. Feridex I.V. may cause severe back, groin, leg, or other pain, or allergic reactions.

3. The infusion fluid is a dark color.

4. The skin surrounding the infusion site may discolor if there is extravasation. The discoloration should disappear over time.

Drug Interactions

Drug interactions were not noted and were not studied in clinical studies. **(See CLINICAL PHARMACOLOGY section on Drug-Drug Interactions.)**

Feridex I.V. administration provides elemental iron. In patients who are receiving supplemental iron orally or parenterally, the dose of supplemental iron may need to be decreased.

The effect of concomitant parenteral iron on Feridex I.V. dosing is not known. **(See CLINICAL PHARMACOLOGY section.)**

LABORATORY TEST FINDINGS

Serum iron levels may be above the normal range following Feridex I.V. administration. Transient increases in serum iron of 15-100% of baseline were observed 18 to 24 hours after Feridex I.V. administration, and returned to normal in most patients by 7 days after administration. Increases in serum ferritin levels were seen 1 to 7 days after administration.

(See CLINICAL PHARMACOLOGY, PHARMACOKINETICS section.)

In a Phase 1 study in normal subjects, PTT was statistically significantly increased; however, all values were within the normal range and no subjects had a more than 40% increase from baseline. In clinical trials of patients who had baseline hematologic abnormalities associated with underlying liver disease, an effect of Feridex I.V. on platelet or PTT was not demonstrated.

In patients with low hematocrit and hemoglobin, over a period of 48 hours to 7 days after Feridex I.V., the serum iron, the hematocrit and hemoglobin levels increase slightly.

CARCINOGENESIS, MUTAGENESIS, AND IMPAIRMENT OF FERTILITY

Long term studies in animals have not been performed to evaluate the carcinogenic potential of Feridex I.V. Therapeutic iron dextran products have been associated with the development of sarcomas at the intramuscular injection sites; the length of treatment or the length of time after injection until development of tumor is not known. Ferumoxides are iron oxides associated with dextran. Whether Feridex I.V. has a risk of tumorigenesis that is similar to that of iron dextran is not known.

Feridex I.V. was not genotoxic in a series of studies that included the Ames test, the CHO/HGPRT forward mutation assay, a chromosome aberration test in CHO cells, an unscheduled DNA synthesis assay, and a micronucleus assay in mice.

Feridex I. V. did not impair the fertility of male or female rats at dosages that were up to approximately 5 times the clinical dose when normalized to body surface area.

PREGNANCY

Teratogenic Effects.

Pregnancy Category C. Feridex I.V. is teratogenic in rabbits at all studied doses. The smallest dose studied was approximately six times the clinical dose when normalized to body surface area. Adequate and well controlled studies were not conducted in pregnant women. Feridex I.V. should be used during pregnancy only if the potential benefit justifies the potential risk.

NURSING MOTHERS

It is not known whether Feridex I.V. is excreted in human milk. This drug should only be used in nursing women if the benefit clearly outweighs the risk.

PEDIATRIC USE

Safety and efficacy of Feridex I.V. in the pediatric population have not been established.

ADVERSE REACTIONS

In clinical trials, a total of 2240 subjects (32 healthy volunteers and 2208 patients with known or suspected liver lesions) received Feridex I.V. Of these subjects, 35% received the recommended dose of 0.56 mg Fe/kg and 62% received a dose of 0.84 mg Fe/kg. Forty-four percent were female and 56% were male, with a mean age of 54.9 years (range 11 - 89).

Of 866 subjects in whom race is known, 647 (75%) were Asian, 199 (22%) were Caucasian, 14 (2%) were Black, 3 (<1%) were Hispanic, and 3 (<1%) other. Racial demographic information was not available for the 1374 subjects in European clinical trials.

Of the 2240 subjects, 197 (8.8%) experienced an adverse event. The most commonly noted adverse experiences were back pain (3.4%), and vasodilation (2.3%).

In a subgroup of 1535 patients in controlled clinical trials, in 44 (2.9%) of the patients [9/226 (3.9%) in US, 10/635 (1.6%) in Japanese, and 25/674 (3.7%) in European studies] the infusion was interrupted or discontinued because of acute, moderate to severe pain (back, lower torso, chest, groin, or upper leg) with or without hypotension. Some patients required treatment. In a few of the patients with pain 11/44 (25%), the infusion was interrupted, restarted, and completed. **(See WARNINGS section.)**

Pain in any location was reported in 4.2% of these 1535 patients given Feridex I.V.

In a subgroup of 689 patients in whom associated underlying disorders were evaluated, back pain occurred in 18/144 (12.5%) patients with cirrhosis and in 10/545 (1.8%) patients who did not have cirrhosis. The frequency of pain in patients with other liver abnormalities is not known.

Anaphylactic and allergic adverse events (e.g., generalized urticaria, respiratory symptoms, and hypotension) that required acute treatment occurred in 11/2240 (0.5%) of patients who received Feridex I.V.

Most other adverse reactions were mild to moderate, of short duration, and resolved spontaneously without treatment. A relationship between adverse events and dose, age, or gender was not observed.

Adverse reactions that occurred in greater than or equal to 0.5% of the 1535 patients in controlled clinical trials are listed below in

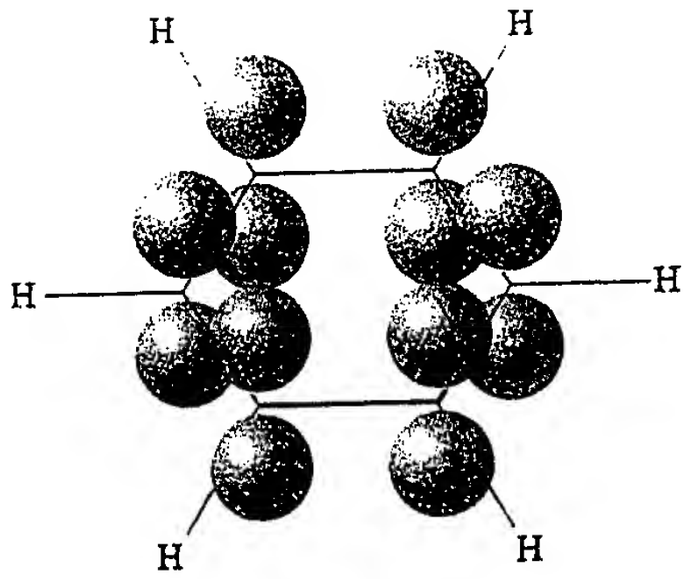

Although the depiction of *p* orbitals in our illustration does not show this, each lobe of each *p* orbital, above and below the ring, overlaps with the lobe of a *p* orbital on each atom on either side of it. This kind of overlap of *p* orbitals leads to a set of bonding molecular orbitals that encompass all of the carbon atoms of the ring. Therefore, the six electrons associated with these *p* orbitals (one from each) are **delocalized** about all six carbon atoms of the ring. This delocalization of electrons explains how all the carbon–carbon bonds are equivalent and have the same length. In Section 14.7B, when we study nuclear magnetic resonance spectroscopy, we shall present convincing physical evidence for this delocalization of the electrons.

When the benzene ring is attached to some other group of atoms in a molecule, it is called a **phenyl group** and it is represented in several ways:

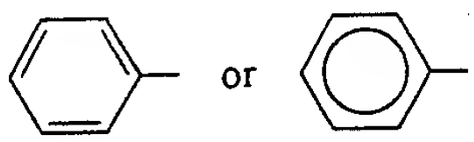 or or C_6H_5— or Ph— or ϕ—

Ways of representing a phenyl group

The combination of a phenyl group and a —CH_2— group is called a **benzyl group.**

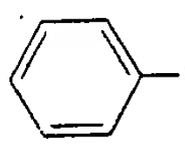 —CH_2— or 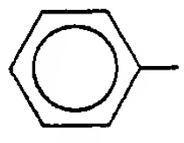 —CH_2— or $C_6H_5CH_2$—

Ways of representing a benzyl group

2.8 FUNCTIONAL GROUPS

One great advantage of the structural theory is that it enables us to classify the vast number of organic compounds into a relatively small number of families based on their structures. (The end papers inside the front cover of this text give the most important of these families.) The molecules of compounds in a particular family are characterized by the presence of a certain arrangement of atoms called a **functional group.**

A functional group is the part of a molecule where most of its chemical reactions occur. It is the part that effectively determines the compound's chemical properties (and many of its physical properties as well). The functional group of an alkene, for example, is its carbon–carbon double bond. When we study the reactions of alkenes in greater detail in Chapter 8, we shall find that most of the chemical reactions of alkenes are the chemical reactions of the carbon–carbon double bond.

The functional group of an alkyne is its carbon–carbon triple bond. Alkanes do

Alkyl halides are classified as being primary (1°), secondary (2°), or tertiary (3°).* ***This classification is based on the carbon atom to which the halogen is directly attached.*** If the carbon ***atom*** that bears the halogen is attached to only one other carbon, the carbon atom is said to be a **primary carbon atom** and the alkyl halide is classified as a **primary alkyl halide.** If the carbon that bears the halogen is itself attached to two other carbon atoms, then the carbon is a **secondary carbon** and the alkyl halide is a **secondary alkyl halide.** If the carbon that bears the halogen is attached to three other carbon atoms, then the carbon is a **tertiary carbon** and the alkyl halide is a **tertiary alkyl halide.** Examples of primary, secondary, and tertiary alkyl halides are the following:

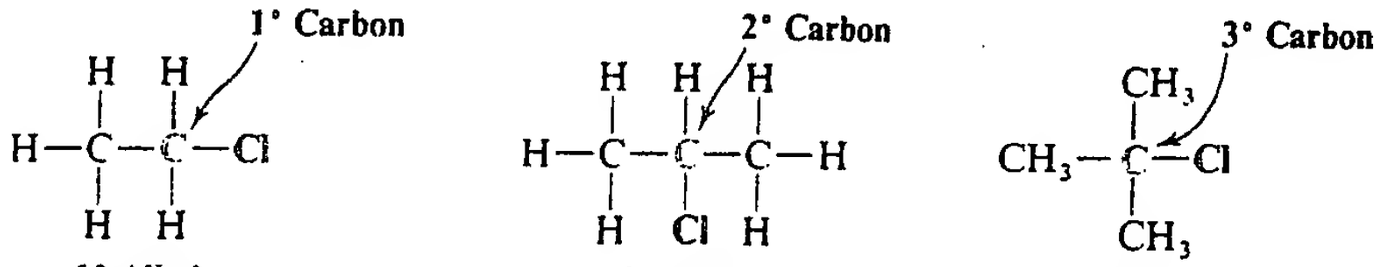

1° Alkyl chloride **2° Alkyl chloride** **3° Alkyl chloride**

PROBLEM 2.4

Write structural formulas (a) for two constitutionally isomeric primary alkyl bromides with the formula C_4H_9Br, (b) for a secondary alkyl bromide, and (c) for a tertiary alkyl bromide with the same formula.

PROBLEM 2.5

Although we shall discuss the naming of organic compounds later when we discuss the individual families in detail, one method of naming alkyl halides is so straightforward that it is worth describing here. We simply name the alkyl group attached to the halogen and add the word *fluoride, chloride, bromide, or iodide.* Write formulas for (a) ethyl fluoride and (b) isopropyl chloride. What are names for (c) $CH_3CH_2CH_2Br$, (d) CH_3CHFCH_3, and (e) C_6H_5I ?

2.10 ALCOHOLS

Methyl alcohol (more systematically called methanol) has the structural formula CH_3OH and is the simplest member of a family of organic compounds known as **alcohols.** The characteristic functional group of this family is the hydroxyl (OH) group attached to a sp^3-hybridized carbon atom. Another example of an alcohol is ethyl alcohol, CH_3CH_2OH (also called ethanol).

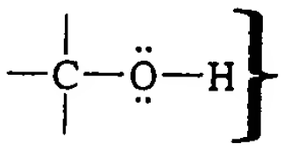

*Although we use the symbols 1°, 2°, 3°, we do not *say* first degree, second degree, and third degree; we say *primary, secondary,* and *tertiary.*

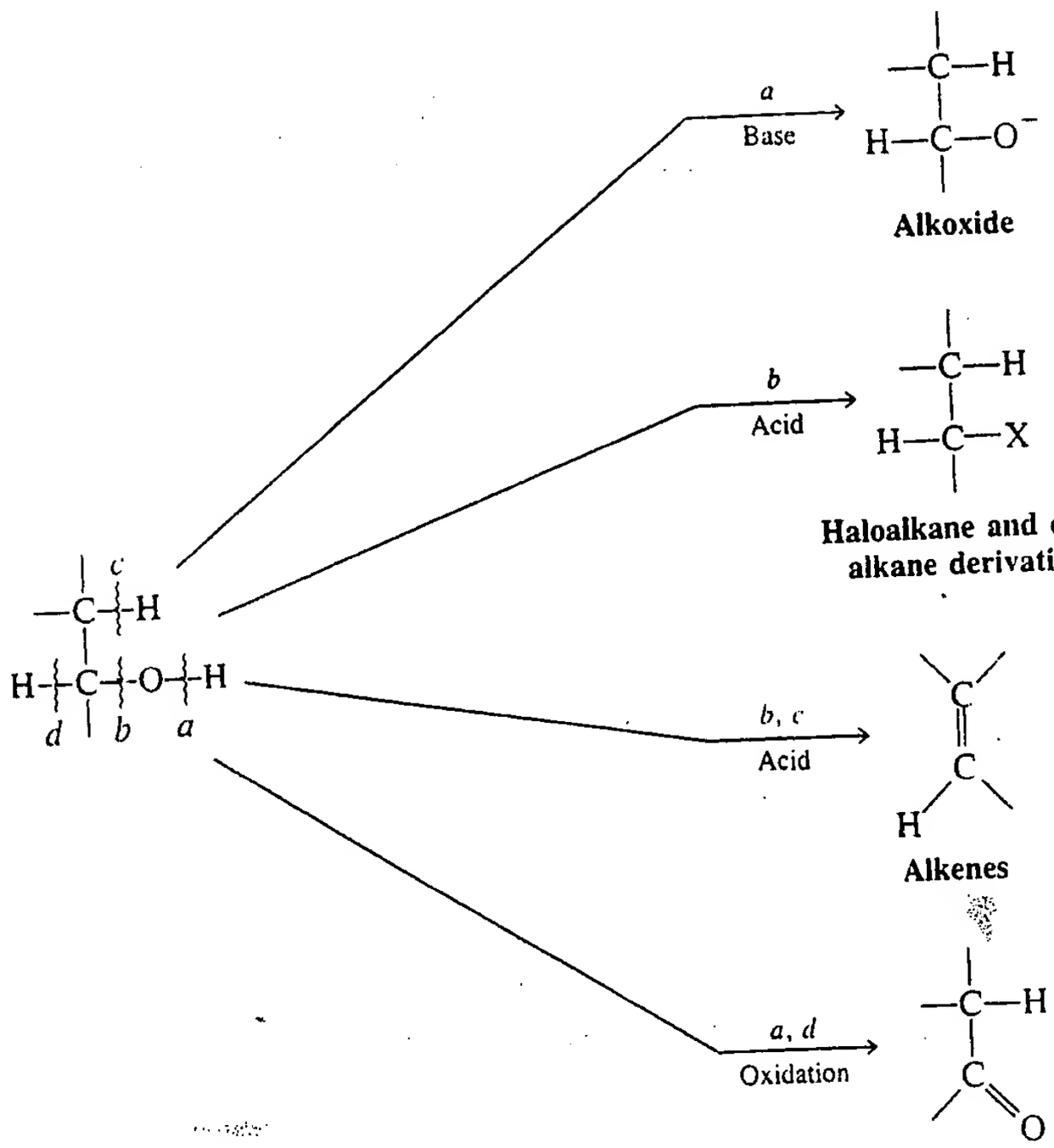

FIGURE 9-1 Four typical reaction modes of alcohols. In each, one or more of the four bonds marked *a*–*d* are cleaved (wavy line denotes bond cleavage): (*a*) deprotonation by base; (*b*) protonation by acid followed by uni- or bimolecular substitution; (*b*, *c*) elimination; and (*a*, *d*) oxidation.

cleavage of bonds *b* and *c*. We shall see that the carbocations arising from acid treatment of secondary and tertiary alcohols have a varied chemistry. An introduction to the preparation of esters and their applications in synthesis is followed by the chemistry of ethers and sulfur compounds. Alcohols, ethers, and their sulfur analogs occur widely in nature and have numerous applications in industry and medicine.

9-1 Preparation of Alkoxides

As described in Section 8-3, alcohols can be both acids and bases. In this section we shall review the methods by which alcohols are deprotonated to furnish their conjugate bases, the alkoxides.

Strong bases are needed to deprotonate alcohols

To remove a proton from the OH group of an alcohol (Figure 9-1, cleavage of bond *a*), we must use a base stronger than the alkoxide. Examples include lithium diisopropylamide, butyllithium, and alkali metal hydrides such as potassium hydride, KH. The latter are particularly useful because the only by-product of the reaction is hydrogen gas.

Three Ways of Making Methoxide from Methanol

$$CH_3OH \;(pK_a = 15.5) + Li^+ {}^-NCH(CH_3)_2 \xrightleftharpoons{K = 10^{24.5}} CH_3O^-Li^+ + HNCH(CH_3)_2 \;(pK_a = 40)$$

$$CH_3OH \;(pK_a = 15.5) + CH_3CH_2CH_2CH_2Li \xrightleftharpoons{K = 10^{34.5}} CH_3O^-Li^+ + CH_3CH_2CH_2CH_2H \;(pK_a = 50)$$

$$CH_3OH \;(pK_a = 15.5) + K^+H^- \xrightleftharpoons{K = 10^{22.5}} CH_3O^-K^+ + H{-}H \;(pK_a = 38)$$

EXERCISE 9-I

Considering the pK_a data in Table 6-4, would you use sodium cyanide as a reagent to convert methanol into sodium methoxide? Explain your answer.

Alkali metals also deprotonate alcohols

Another common way to obtain alkoxides is by the reaction of alcohols with alkali metals. Such metals reduce water—in some cases, violently—to yield alkali metal hydroxides and hydrogen gas. When the more reactive metals (sodium, potassium, cesium) are exposed to water in air, the hydrogen generated can ignite spontaneously or even detonate.

$$2\ H{-}OH + 2\ M\ (Li, Na, K) \longrightarrow 2\ M^+\ {}^-OH + H_2$$

The alkali metals act similarly on the alcohols to give alkoxides, but the transformation is less vigorous. Here are two examples.

Alkoxides from Alcohols and Alkali Metals

$$2\ CH_3CH_2OH + 2\ Na \longrightarrow 2\ CH_3CH_2O^-Na^+ + H_2$$
$$2\ (CH_3)_3COH + 2\ K \longrightarrow 2\ (CH_3)_3CO^-K^+ + H_2$$

The reactivity of the alcohols used in this process decreases with increasing substitution, methanol being most reactive and tertiary alcohols least reactive.

Relative Reactivity of ROH with Alkali Metals

$$R = CH_3 > \text{primary} > \text{secondary} > \text{tertiary}$$

2-Methyl-2-propanol reacts so slowly that it can be used to safely destroy potassium residues in the laboratory.

What are alkoxides good for? We have already seen that they can be useful reagents in organic synthesis. For example, the reaction of hindered alkoxides with haloalkanes gives elimination.

$$CH_3CH_2CH_2CH_2Br \xrightarrow{(CH_3)_3CO^-K^+;\ (CH_3)_3COH} CH_3CH_2CH{=}CH_2 + (CH_3)_3COH + K^+Br^-$$

Less branched alkoxides attack primary haloalkanes by the S_N2 reaction to give ethers. This method is described in Section 9-6.

Exhibit 14

Ralph Weissleder, MD, PhD • Guillermo Elizondo, MD • Jack Wittenberg, MD • Carlos A. Rabito, MD, PhD • Howard H. Bengele, PhD • Lee Josephson, PhD

Ultrasmall Superparamagnetic Iron Oxide: Characterization of a New Class of Contrast Agents for MR Imaging[1]

An ultrasmall superparamagnetic iron oxide (USPIO) preparation was developed that is small enough to migrate across the capillary wall, a prerequisite in the design of targetable particulate pharmaceuticals. Seventy percent of particles were smaller than 10 nm; 26%, smaller than 5 nm. The blood half-life of USPIO in rats was 81 minutes, considerably longer than that of larger superparamagnetic iron oxide preparations such as AMI-25 (6 minutes). Electron microscopy demonstrated that USPIO particles transmigrate the capillary wall by means of vesicular transport and through interendothelial junctions. Twenty-four hours after intravenous administration, 3.6% of the injected dose per gram of tissue was found in lymph nodes, 2.9% per gram in bone marrow, 6.3% per gram in liver, and 7.1% per gram in spleen. The major potential applications for USPIO are as (*a*) an intravenous contrast agent for the lymphatic system, (*b*) a bone marrow contrast agent, (*c*) a long-half-life perfusion agent for brain and heart, and (*d*) the magnetic moiety in organ-targeted superparamagnetic contrast agents for magnetic resonance imaging.

Index terms: Iron • Magnetic resonance (MR), contrast enhancement

Radiology 1990; 175:489–493

CONVENTIONAL superparamagnetic iron oxide particles of 30–1,000-nm diameter have been used to enhance relaxation times of liver and spleen (1–5). After intravenous administration, all of these agents are cleared from the blood within minutes, rapidly accumulating in cells of the mononuclear phagocytic system (MPS) of liver and spleen; however, virtually no particles are found in other tissues (6). We have developed an intravenous ultrasmall superparamagnetic iron oxide (USPIO) that is not immediately recognized by the MPS of liver and spleen and thus has a longer blood half-life. The small size and prolongation of the plasma half-life enables this agent to cross the capillary wall and have more widespread tissue distribution, including uptake by the MPS of lymph nodes and bone marrow.

Herein, we report the physical properties, pharmacologic behavior, and results of vascular permeability studies of USPIO. A subsequent study (7) describes the results of intravenous administration of USPIO to enhance the detection of lymph node metastases in an animal model with magnetic resonance (MR) imaging.

MATERIALS AND METHODS

Iron Oxide Preparations

USPIO, obtained through size fractionation of a heterogeneous iron oxide preparation (AMI-25; Advanced Magnetics, Cambridge, Mass) with use of a sephadex gel chromatography column (Pharmacia LKB Biotechnology, Piscataway, NJ), was supplied by Advanced Magnetics. The smallest 10%–15% of the iron oxide particles eluted through the column was separated and concentrated by ultrafiltration to obtain an iron concentration of 8.4 mg/mL. USPIO has an apparent molecular weight by gel filtration of approximately 700,000 d, similar to that of endogenous ferritin (11 nm; molecular weight, 440,000–600,000 (8). Labeled USPIO was obtained in an identical fashion through fractionation of iron-59–labeled AMI-25.

Control studies were performed with a standard iron oxide preparation (AMI-25). AMI-25 was prepared as described previously (9) and was provided as a stable aqueous colloid with an iron concentration of 11.2 mg/mL (200 μmol/mL). AMI-25 has a volume median diameter of 72 nm as measured by means of laser light scattering on a BI-90 particle size analyzer (Brookhaven Instruments, Ronkonkoma, NY). The relaxivities of this preparation were 23.9 and 98.3 $(mmol/L \cdot sec)^{-1}$ respectively, for R1 and R2, as determined in water. Radioactive AMI-25 was synthesized with Fe-59 incorporated into the superparamagnetic iron oxide core. The specific activity was 8,460 μCi (313 MBq) per micromole of iron at calibration. The radiolabeled particles were mixed with unlabeled particles to give a specific activity of 36 μCi (1.3 MBq) per micromole of iron (6).

Organ biodistribution in rats was determined by injection of Fe-59–labeled USPIO at a dose of 40 μmol of iron per kilogram. Animals were killed 1 or 24 hours after injection. Animals were exsanguinated and tissues blotted dry. Thereafter, tissues were weighed and placed in 1.5-mL microcentrifuge tubes. All tissue samples were counted with a high-efficiency Fe-59 gamma counter (Packard Auto-Gamma Scintillation Spectrometer; Hewlett-Packard, Chicago). Radioactivity was corrected at each time point for Fe-59 decay, and results were expressed as the percentage of the injected dose per organ and per gram of tissue. Values were expressed as means and standard errors of the mean (SEMs).

Magnetic Characterization

The magnetic behavior of USPIO was evaluated at 25°C with a vibrating sample magnetometer (model 155; Princeton Applied Research, Princeton, NJ). Prior to measurements, samples were dried by lyophilization. The iron content of the ly-

[1] From the Department of Radiology, Massachusetts General Hospital and Harvard Medical School, 32 Fruit St, Boston, MA 02114 (R.W., J.W., C.R.); the Nuclear Magnetic Resonance Unit, University Hospital, Monterrey, Mexico (G.E.); and Advanced Magnetics, Inc, Cambridge, Mass (H.H.B., L.J.). Received October 17, 1989; revision requested December 11; revision received December 28; accepted January 11, 1990. Address reprint requests to R.W.

See also the other article by Weissleder et al (pp 494–498) in this issue.

Abbreviations: MPS = mononuclear phagocytic system, SEM = standard error of the mean, USPIO = ultrasmall superparamagnetic iron oxide.

ophilized sample was determined by atomic adsorption spectrophotometry after digestion with 0.1 N hydrochloric acid.

Electron Microscopy

The following experiments were designed to gain insight into the ultrastructural pathways and loci of action of USPIO. Rats were injected with USPIO at a dose of 200 μmol of iron per kilogram and killed after 15 minutes, 1 hour, or 24 hours. Tissues with known types of different capillaries (high endothelial venules in the lymph nodes, fenestrated capillaries in the jejunum, continuous capillaries in muscle) were fixed in situ by perfusion with cold fixative and then studied by means of electron microscopy without prior staining. The fixative (2.5% glutaraldehyde in 0.1 mol/L cacodylate buffer with 1 mmol/L $CaCl_2$ at pH 7.4, cooled at 3°C) was always perfused through the vascular system, instilled around the tissue to be excised, dripped into the abdominal cavity, or injected into the bowel lumen to avoid fixation artifacts.

After removal and successive dehydration in graded alcohols, the specimens were embedded in Epon and sectioned with an ultratome at 60-nm thickness without prior staining. Electron microscopy was performed on a Jeol (Palo Alto, Calif) JEM100S. The voltage was 60 kV. Micrographs were taken at initial magnifications of ×3,000 to ×100,000 and enlarged photographically 2.6 times.

To determine the size distribution of USPIO, 0.1 g of agar (Sigma Chemical, St Louis) was dissolved in 10 mL of boiling fixation buffer (2.5% glutaraldehyde in 0.1 mol/L cacodylate buffer with 1 mmol/L $CaCl_2$ at pH 7.4) and maintained in a water bath at 45°C. The molten agar was then mixed in a 1:1 ratio with ferritin (Sigma) as a positive control or with USPIO. Mixtures were stirred rapidly with a vortex mixer and then poured onto a cold microscope slide. The blocks of agar were treated as in routine fixation and processed for electron microscopy. Micrographs were enlarged 100,000 times, and the largest diameter of a total of 200 individual particles in each specimen was determined.

Endothelial Monolayer Experiments

The vascular endothelium is the primary barrier in the transport of macromolecules from the vascular lumen into the interstitium. Cultured endothelial cell monolayers have been used to quantitate transcytosis of biologic macromolecules (diameter, 2–10 nm) across endothelial cells by determining the amount of radioactively marked tracer in a chamber-well experiment (10,11).

We used an endothelial cell system originally obtained from the microvasculature of pig glomeruli (11). These cells have been extensively characterized and are preferred for transcytosis experiments because of their peripheral rather than central arterial or venous origin. The cell culture medium was changed 1–2 days after initial seeding to remove excess blood and thereafter was changed every 5 days. After five to 10 population doublings, cells were removed from the flask (Dow-Corning, Corning, NY) through trypsination. The endothelial monolayer was then grown on polycarbonate filters coated with collagen to divide a well into a two-compartment system consisting of luminal and abluminal chambers (13-mm diameter, 10-μm thickness, 3.0-μm pore diameter) (Costar, Cambridge, Mass). Each collagen-coated filter was seeded with 2×10^5 cells in 0.5 mL. The wells were incubated at 37°C in a 95% air and 5% carbon dioxide atmosphere and used 72 hours after seeding. The medium used in both compartments was Dulbecco modified Eagle medium, with fraction V bovine serum albumin (0.5 g/dL) and hydroxyethylpiperazine ethanosulfonic acid (20 mmol/L) at a pH of 7.4. Studies were performed by adding Fe-59–labeled particle preparations to the luminal chamber; an equal volume of phosphate-buffered saline (0.01 mol/L) was used in negative control studies. Both chambers were sampled every 5 minutes for 1 hour, and the clearance rate was calculated from these data points.

Relaxation Time Measurements

T1 and T2 relaxation times were measured in milliseconds with an MR spectrometer operating at 0.47 T and at 37°C (PC-20 Minispec; IBM, Danbury, Conn). Before the measurements were made, the spectrometer was tuned and calibrated. T1 was measured from eight data points generated by an inversion-recovery pulse sequence. T2 was measured from 10 data points generated by a Carr-Purcell-Meiboom-Gill pulse sequence with a tau of 1 msec.

To determine the relaxivity of USPIO, solutions of increasing concentrations were prepared and their relaxation times measured. T1 and T2 relaxation times were expressed as the inverse (1/T1, 1/T2) and plotted against the concentration. The slopes of these two curves correspond to R1 and R2 relaxivity. In all experiments, the linear correlation coefficient *r* of the curve fit was larger than 0.9 (12).

Blood half-lives of USPIO and AMI-25 were calculated after intravenous injections into Sprague-Dawley rats at doses of 40 μmol of iron per kilogram. Blood samples were drawn at multiple intervals of up to 4 hours from six different animals (half-lives were expressed as means ± SEMs). Blood relaxation times were determined at 37°C. Blood half-life was calculated by fitting mean 1/T1 values of blood to a single exponential equation: $1/T1_t = 1/T1_{t0} + Ce^{-kt}$, where $1/T1_{t0}$ is the spin-lattice relaxation rate of blood before injection of the colloid, $1/T1_t$ is the relaxation rate at time *t* after injection, C is the concentration of the colloid in the blood at the moment of injection, and *k* is the rate constant for the decay.

Biodistribution of Fe-59-Labeled USPIO

Tissue	Uptake	
	1 Hour	24 Hours
Spleen	4.50 ± 0.37	7.12 ± 0.57
Liver	4.39 ± 0.17	6.32 ± 0.22
Lymph nodes	1.04 ± 0.19	3.62 ± 0.64
Marrow	1.13 ± 0.07	2.91 ± 0.18
Thyroid	0.10 ± 0.03	0.05 ± 0.00
Muscle	0.01 ± 0.00	0.01 ± 0.00

Note.—Normal Sprague-Dawley rats received doses of 40 μmol of iron per kilogram (2 μCi [0.074 MBq] per rat) and were killed after 1 hour ($n = 5$) or after 24 hours ($n = 6$). Values are given as the percentage of the injected dose per gram of tissue for each organ (mean ± SEM). The lymph node fraction contains iliac, celiac, paraaortic, mesenteric, and mediastinal nodes.

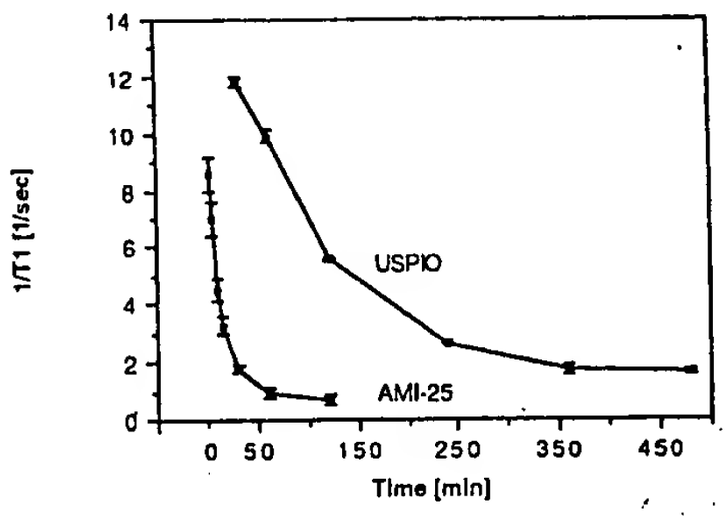

Figure 1. Blood clearance of USPIO and AMI-25. Means and SEMs of data from six animals are shown for each contrast medium. The calculated blood half-life of USPIO was 81 minutes, and that of AMI-25 was 6 minutes.

Animals

Male Sprague-Dawley rats (Charles River Laboratories, Wilmington, Mass) weighing 200–300 g were used for all experiments. Six animals were used for selective perfusion experiments, six for determination of blood half-life, 10 for electron microscopy studies, and 11 for Fe-59-labeled USPIO biodistribution studies.

Selective Perfusion Experiments

To determine the pathways of USPIO accumulation in lymph nodes (extravasation through nodal capillaries or transportation to nodes through afferent lymphatic vessels after extravasation through peripheral capillaries throughout the body), the following selective perfusion experiments were performed. In one group of animals ($n = 3$), afferent lymphatic vessels of popliteal lymph nodes were occluded under an operating microscope (Zeiss, Wetzlar, Federal Republic of Germany) while the nodal vascular pedi-

a. b.

Figure 2. Electron micrographs of transcapillary passage. Electron microscopy was performed in fenestrated bowel capillaries (**a**) and high endothelial venules (**b**) at 1 hour after administration of USPIO (200 μmol of iron per kilogram). Fixation in situ was performed in all specimens; note that the sections are unstained to allow easier detection of electron-dense iron oxide particles. (**a**) Section through a bowel capillary (original magnification, ×100,000) demonstrates the vascular lumen (*L*) and the capillary wall (*W*). Several USPIO particles are seen in the vascular lumen as well as within an endothelial vesicle (arrow), transcytosing into the interstitial space. (**b**) Transmission electron micrograph (original magnification, ×20,000) of a high endothelial venule within a lymph node demonstrates a lymphocyte (*L*) in the vascular lumen. At high-power magnification (inset) (original magnification, ×100,000), several high-density USPIO particles can be seen in vesicles in the capillary wall (curved arrow) and in interendothelial junctions (straight arrow) leaving the vascular space.

cle was left intact. In a second group of animals (n = 3), popliteal lymphatic arterioles were selectively ablated and afferent lymphatics were kept intact. In both groups, USPIO was then injected into the vena cava. Two hours later, popliteal lymph nodes were resected and processed for histologic iron stains.

Statistical Analysis

Differences in blood half-lives between USPIO and AMI-25 were evaluated statistically by means of the nonparametric Wilcoxon test (13).

RESULTS

Physical Properties

Magnetic properties.—The T1 relaxivity (R1) of USPIO was 21.6 $(mmol/L \cdot sec)^{-1}$ and the T2 relaxivity (R2) was 44.1 $(mmol/L \cdot sec)^{-1}$, where mmol/L is the millimolar concentration of iron (37°C, 0.47 T). As is expected for very small superparamagnetic particles, the R2/R1 ratio was approximately 2, lower than that of larger iron oxide particles (12). The hysteresis curve showed saturation of the dried USPIO preparation at 0.6 T with an induced magnetization of 60 emu per gram of iron. Typical of all superparamagnetic preparations, there was no remnant magnetization after the applied magnetic field was turned off (0 emu per gram of iron at 0 T).

Size distribution.—The mean particle size of USPIO was 11.4 nm ± 6.3, and of ferritin, 9.3 nm ± 3.6. Although USPIO showed a more heterogeneous size distribution (larger standard deviation) than ferritin, 26% of USPIO particles were smaller than 5 nm, 70% were smaller than 10 nm, 96% were smaller than 20 nm, and 100% were smaller than 30 nm. The particle size of ferritin as measured in these electron microscopy experiments corresponds well to the reported mean size of 11 nm found by other investigators (8).

Pharmacology

Biodistribution.—Fe-59–labeled USPIO particles were used to determine the uptake in lymph nodes and other tissues. At 1 and 24 hours after intravenous administration of 40 μmol of iron per kilogram, 0.33% ± 0.04% (mean ± SEM) and 0.79% ± 0.10% of the dose, respectively, were found in lymph nodes. Remaining radioactivity was found in the liver (66.1% ± 2.27%), spleen (5.15% ± 0.51%), and carcass.

When concentration is expressed as percentage of the injected dose per gram of tissue, abdominal, pelvic, and mediastinal lymph nodes (3.62% ± 0.64%) show approximately half the concentration found in the liver (6.32% ± 0.22%) and spleen (7.12% ± 0.57%) after 24 hours (Table). In contrast, larger superparamagnetic particles, such as AMI-25, show rapid and nearly exclusive clearance by the liver and spleen with virtually no uptake by the nodes (14). The concentration of USPIO in bone marrow was 2.91% ± 0.18%. Thyroid and muscle showed virtually no uptake of the label (Table).

Blood half-life.—The blood half-life of the T1 effect of USPIO in rats was 81 minutes (Fig 1). This half-life is significantly longer ($P < .001$) than that of the conventional superparamagnetic iron oxide preparation (AMI-25, 6 minutes), indicating that USPIO particles are less readily recognized, opsonized, and/or phagocytosed by the MPS of the liver and spleen. This extended intravascular duration creates the potential for transcytosis through the capillary wall, thereby resulting in interstitial distribution.

Vascular Permeability

Electron microscopy.—USPIO could be regularly identified within endothelial vesicles of fenestrated (bowel) and continuous capillaries (muscle) (Fig 2). Intravesicular and interstitial distributions of transcytosed particles in and around fenestrated and continuous capillaries were similar to those observed by other authors after the administration of ferritin (8,15,16). Within lymph nodes, particle intravasation into nodal parenchyma through high endothelial venules was demonstrated. Electron-dense particles were observed in nodal macrophages within 1 hour after administration of USPIO. Twen-

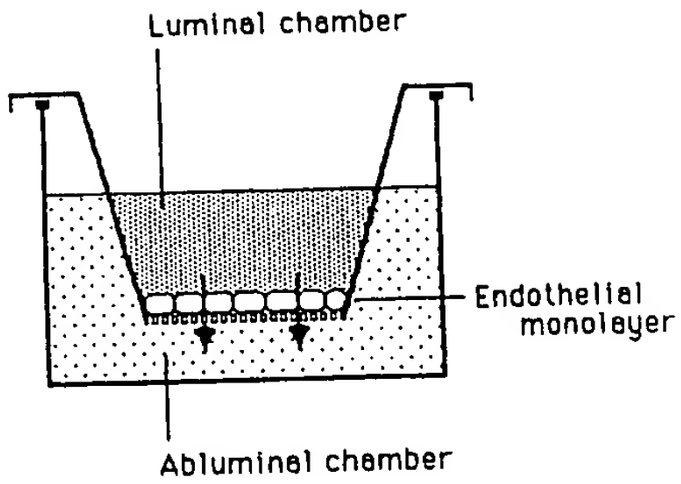

a.

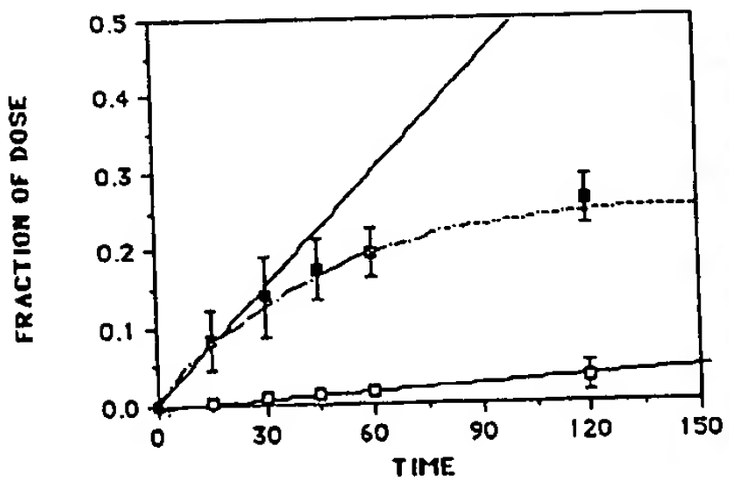

b.

Figure 3. Sieving characteristics through endothelial monolayer. Transcytosis of USPIO and AMI-25 control particles were studied in an endothelial monolayer model. **(a)** Continuous layer of endothelial cells was grown on a porous collagenized carbon fiber mesh to separate a well into abluminal and luminal chambers. The integrity of the cell layer was confirmed by means of ion conductance methods. Both iron oxide particle species were labeled with Fe-59 and pipetted into the well insert (luminal chamber). Sampling of Fe-59–labeled iron oxide particles on the other side of the endothelial layer (abluminal chamber) was performed at 15-minute intervals. **(b)** Graph shows the accumulations over time of USPIO (■) and control particles (□) in the abluminal chambers. Each data point represents the mean and standard deviation from four individual monolayer experiments. At 120 minutes, there is less transcytosis (power log curve), as nutrients in the closed system are limited. At even longer intervals, cells would die and radioactivity would come to an equilibrium between the well and the abluminal chamber. For these reasons, permeability is calculated from the tangent to the first 15-minute time point (linear line) and extrapolated to 1 hour. The permeability ratio of USPIO to conventional particles is 46:1.

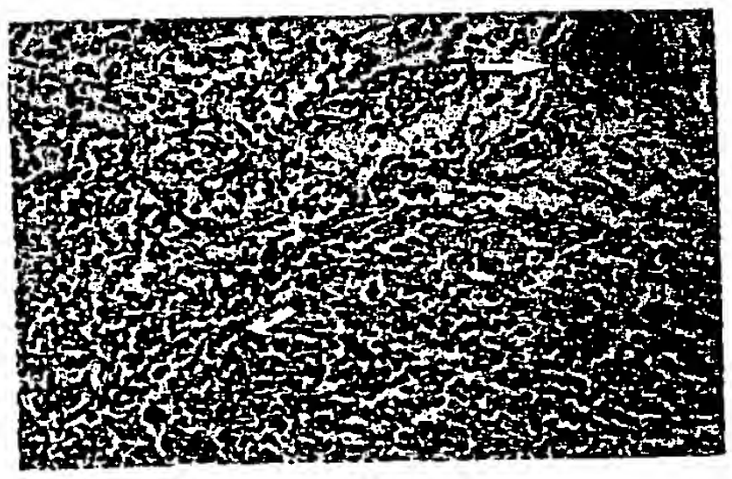

Figure 4. Selective perfusion of lymphatic capillary with USPIO. **(a)** Arterioles of this lymph node were selectively perfused with USPIO after ablation of afferent lymphatic vessels. One hour after administration, the node was fixed and stained with Prussian blue for iron. Note that there is still faint blue pigment in the vessel (straight arrow), indicating the long blood half-life of USPIO. Blue stain is also seen in sinuses and in macrophages (curved arrow), indicative of intranodal extravasation.

ty-four hours after administration, all particles had accumulated in macrophage phagolysosomes and no cytoplasmatic distribution was noted.

Endothelial monolayer sieving characteristics.—Monolayers of cultured endothelial cells were used as an in vitro system to model an in vivo capillary wall and measure the transcytotic flux of Fe-59–labeled USPIO and AMI-25 (Fig 3). The amount of USPIO (fraction of dose initially injected into well) recovered in the abluminal chamber was 45.4% ± 10.9% after 5.5 hours. In comparison, only 10.9% ± 4.4% of AMI-25 was found on the abluminal side at that time point (Fig 3). Because of the closed two-compartment system, the curves show an exponential rather than linear behavior; permeability of particulates through endothelial monolayers is therefore traditionally calculated from the tangent through the 15-minute time point. With use of four individual experiments for each iron oxide preparation, the permeabilities of USPIO and AMI-25, respectively, were 0.066 and 0.0032 mg Fe/h · cm^2. The permeability ratio of 46:1 indicates that flux across endothelial monolayers is steeply dependent on particle diameter.

Selective lymph node perfusion experiments.—In animals with obliterated afferent lymphatic vessels, USPIO was found in macrophages and sinuses throughout the lymph nodes (Fig 4). This finding indicates that lymphatic vascular capillaries are permeable to USPIO. In the second group of animals in which lymph node arterioles were selectively ablated, small amounts of USPIO were identified in macrophages located in the marginal sinus. This finding implies that a second pathway must exist for lymphatic accumulation of USPIO, presumably capillary extravasation into the interstitium throughout the body and subsequent uptake by draining lymphatic vessels with ultimate transport to lymph nodes.

DISCUSSION

Previous reports demonstrate rapid uptake of superparamagnetic iron oxides by the MPS of liver and spleen. The present study demonstrates that biodistribution can be altered by reducing the size of the particles. We originally hypothesized that a small enough superparamagnetic iron oxide colloid might follow the normal transendothelial pathways established for large macromolecules, while still being large enough to be recognized by the MPS of lymph nodes. Indeed, our current results verify the hypothetical predictions that USPIO can be delivered to the interstitium by nonspecific vesicular transport and through transendothelial channels. Once in the interstitium, USPIO particles are cleared by draining lymphatic vessels and transported to lymph nodes. USPIO particles also reach lymph nodes directly through interendothelial junctions of high endothelial venules, specific vessels where the homing (vascular-nodal exchange) of lymphocytes occurs.

The endothelial permeability of particulates has been subject to multiple studies (17,18). Physiologically, permeability of the capillary wall can be rationalized in terms of one or two pore systems of different pore size and density. The most widely accepted concept is that there are two pore sizes, small (9 nm) and large (50–70 nm) (17). By means of electron microscopy, at least four morphologic correlates of outward pathways of particulates have been found: open interendothelial junctions, vesicular transport, open transendothelial channels, and open and closed fenestrae (18). A variety of electron-dense tracers have been used to study vascular permeability (16,17,19). The USPIO particles used in this study have dimensions similar to these probes. For example, ferritin, a prototype electron-dense tracer, has been demonstrated in the adventitia and pericapillary spaces of muscle within 5–10 minutes after intravenous injection (15). Although the interstitial concentration of ferritin is initially exceedingly low, it increases slowly to approach that in the vascular lumen by 24 hours. The total amount of ferritin particles that move from plasma to interstitial fluid is high (20). Theoretical calculations based on the quantitative results of transcytosis experiments (16) show that one single capillary may allow transendothelial transport of up to 10^6 particles into the interstitium every 10 minutes.

Our results suggest that superparamagnetic iron oxide particles may be synthesized in the size range of plasma proteins without substantially reducing relaxation properties and while maintaining a relatively long blood half-life. Although half-lives on the order of 60 minutes have been reported for small liposome preparations (21,22), no iron oxide particle with a half-life similar to that of USPIO has previously been synthesized. Such properties indicate that USPIO should have several potential future clinical applications, including use as (*a*) an intravenous agent with specificity for lymph nodes (7), (*b*) a bone marrow imaging agent, (*c*) a perfusion agent for MR imaging of brain and heart, and (*d*) a magnetic core in tissue-specific pharmaceuticals. The specific application of USPIO as an intravenous contrast agent for the detection of lymphatic malignancy with MR imaging is the subject of a different study (7). Future studies are warranted to determine the exact pharmacokinetics, in vivo relaxation effects, and toxicity of USPIO. ■

References

1. Magin R, Bacic G, Alameda J, Neisman M, Wright S, Swartz H. Dextran magnetite as a liver contrast agent. In: Book of abstracts: Society of Magnetic Resonance in Medicine 1988. Berkeley, Calif: Society of Magnetic Resonance in Medicine, 1988; 538.
2. Widder D, Greif W, Widder K, Edelman R, Brady T. Magnetite albumin microspheres: a new MR contrast material. AJR 1987; 148:399–404.
3. Saini S, Stark D, Hahn P, Wittenberg J, Brady T, Ferrucci J. Ferrite particles: a superparamagnetic MR contrast agent for the reticuloendothelial system. Radiology 1987; 162:211–216.
4. Hemmingson A, Carlsten J, Ericsson A, Klaveness J, Spreber G, Thuomas K. Relaxation enhancement of the dog liver and spleen by biodegradable superparamagnetic particles in proton magnetic resonance imaging. Acta Radiol 1987; 28:703–705.
5. Weissleder R, Hahn P, Stark D, et al. Superparamagnetic iron oxide: enhanced detection of focal splenic tumors with MR imaging. Radiology 1988; 169:399–403.
6. Weissleder R, Stark D, Engelstad B, et al. Superparamagnetic iron oxide: pharmacokinetics and toxicity. AJR 1989; 152:175–180.
7. Weissleder R, Elizondo G, Wittenberg J, Lee AS, Josephson L, Brady TJ. Ultrasmall superparamagnetic iron oxide: an intravenous contrast agent for assessing lymph nodes with MR imaging. Radiology 1990; 175:494–498.
8. Clough G, Michel C. The role of vesicles in the transport of ferritin through frog endothelium. J Physiol 1981; 315:127–142.
9. Groman E, Josephson L, Lewis J. U.S. Patent 4,827,945, 1989.
10. Siflinger-Birnboim A, Cooper J, DelVecchio P, Lum H, Malik A. Selectivity of the endothelial monolayer: effects of increased permeability. Microvasc Res 1988; 36:216–227.
11. Rabito C, Kreisberg J, Wight D. Alkaline phosphatase and gamma-glutamyl transpeptidase as polarization markers during organization of LCC-PK1 cells into an epithelial membrane. J Biol Chem 1984; 259:574–582.
12. Josephson L, Lewis J, Jacobs P, Hahn P, Stark D. The effects of iron oxides on proton relaxivity. Magn Reson Imaging 1988; 6:647–653.
13. Armitage P, Berry G. Statistical methods in medical research. Oxford, England: Blackwell Scientific, 1987.
14. Weissleder R, Elizondo G, Josephson L, et al. Experimental lymph node metastases: enhanced detection with MR lymphography. Radiology 1989; 171:835–839.
15. Bruns R, Palade G. Studies on blood capillaries. II. Transport of ferritin molecules across the wall of muscle capillaries. J Cell Biol 1968; 37:277–299.
16. Simionescu N, Simionescu M, Palade G. Permeability of muscle capillaries to small heme-peptides: evidence for the existence of patent transendothelial channels. J Cell Biol 1975; 64:586–607.
17. Renkin E, Curry F. Endothelial permeability: pathways and modulations. Ann NY Acad Sci 1982; 401:248–259.
18. Simionescu M, Ghitescu L, Fixman A, Simionescu N. How plasma macromolecules cross the endothelium. NIPS 1987; 2:97–100.
19. Simionescu N, Palade G. Dextrans and glycogens as particulate tracers for studying capillary permeability. J Cell Biol 1971; 50:616–624.
20. Palade G, Simionescu M, Simionescu N. Structural aspects of the permeability of the microvascular endothelium. Acta Physiol Scand 1979; 463(suppl):11–32.
21. Gregoriadis G, Senior J, Poste G. Targeting of drugs with synthetic systems. New York: Plenum, 1986.
22. Gabizon A, Papahadjopoulos D. Liposome formulations with prolonged circulation time in blood and enhanced uptake by tumors. Proc Natl Acad Sci 1988; 85:6949–6953.

Exhibit I

- Muldoon, L. L., Pagel, M. A., Kroll, R. A., Roman-Goldstein, S., Jones, R. S., Neuwelt, E. A. (1999). A Physiological Barrier Distal to the Anatomic Blood-Brain Barrier in a Model of Transvascular Delivery. *AJNR Am J Neuroradiol* 20: 217-222 [Abstract] [Full Text]
- Staatz, G., Nolte-Ernsting, C. C. A., Adam, G. B., Grosskortenhaus, S., Misselwitz, B., Bucker, A., Gunther, R. W. (2001). Interstitial T1-weighted MR Lymphography: Lipophilic Perfluorinated Gadolinium Chelates in Pigs. *Radiology* 220: 129-134 [Abstract] [Full Text]
- Kanno, S., Lee, P. C., Dodd, S. J., Williams, M., Griffith, B. P., Ho, C. (2000). A novel approach with magnetic resonance imaging used for the detection of lung allograft rejection. *J Thorac Cardiovasc Surg* 120: 923-934 [Abstract] [Full Text]
- Schmitz, S. A., Winterhalter, S., Schiffler, S., Gust, R., Wagner, S., Kresse, M., Coupland, S. E., Semmler, W., Wolf, K.-J. (2001). USPIO-enhanced Direct MR Imaging of Thrombus: Preclinical Evaluation in Rabbits. *Radiology* 221: 237-243 [Abstract] [Full Text]
- Kanno, S., Wu, Y.-J. L., Lee, P. C., Dodd, S. J., Williams, M., Griffith, B. P., Ho, C. (2001). Macrophage Accumulation Associated With Rat Cardiac Allograft Rejection Detected by Magnetic Resonance Imaging With **Ultrasmall Superparamagnetic Iron Oxide** Particles. *Circulation* 104: 934-938 [Abstract] [Full Text]
- Moore, A., Marecos, E., Bogdanov, A. Jr, Weissleder, R. (2000). Tumoral Distribution of Long-circulating Dextran-coated Iron Oxide Nanoparticles in a Rodent Model. *Radiology* 214: 568-574 [Abstract] [Full Text]

Radiology, Vol 175, 489-493, Copyright © 1990 by Radiological Society of North America

ARTICLES

Ultrasmall superparamagnetic iron oxide: characterization of a new class of contrast agents for MR imaging

R Weissleder, G Elizondo, J Wittenberg, CA Rabito, HH Bengele and L Josephson
Department of Radiology, Massachusetts General Hospital, Boston.

An **ultrasmall superparamagnetic iron oxide** (USPIO) preparation was developed that is small enough to migrate across the capillary wall, a prerequisite in the design of targetable particulate pharmaceuticals. Seventy percent of particles were smaller than 10 nm; 26%, smaller than 5 nm. The blood half-life of USPIO in rats was 81 minutes, considerably longer than that of larger superparamagnetic iron oxide preparations such as AMI-25 (6 minutes). Electron microscopy demonstrated that USPIO particles transmigrate the capillary wall by means of vesicular transport and through interendothelial junctions. Twenty-four hours after intravenous administration, 3.6% of the injected dose per gram of tissue was found in lymph nodes, 2.9% per gram in bone marrow, 6.3% per gram in liver, and 7.1% per gram in spleen. The major potential applications for USPIO are as (a) an intravenous contrast agent for the lymphatic system, (b) a bone marrow contrast agent, (c) a long-half-life perfusion agent for brain and heart, and (d) the magnetic moiety in organ-targeted superparamagnetic contrast agents for magnetic resonance imaging.

This article has been cited by other articles:

- Ahlström, K. H., Johansson, L. O., Rodenburg, J. B., Ragnarsson, A. S., Åkeson, P., Börseth, A. (1999). Pulmonary MR Angiography with **Ultrasmall Superparamagnetic Iron Oxide** Particles as a Blood Pool Agent and a Navigator Echo for Respiratory Gating: Pilot Study. *Radiology* 211: 865-869 [Abstract] [Full Text]
- Schmitz, S. A., Albrecht, T., Wolf, K.-J. (1999). MR Angiography with Superparamagnetic Iron Oxide: Feasibility Study. *Radiology* 213: 603-607 [Abstract] [Full Text]
- Ruehm, S. G., Corot, C., Vogt, P., Kolb, S., Debatin, J. F. (2001). Magnetic Resonance Imaging of Atherosclerotic Plaque With Ultrasmall Superparamagnetic Particles of Iron Oxide in Hyperlipidemic Rabbits. *Circulation* 103: 415-422 [Abstract] [Full Text]
- Turetschek, K., Huber, S., Floyd, E., Helbich, T., Roberts, T. P. L., Shames, D. M., Tarlo, K. S., Wendland, M. F., Brasch, R. C. (2001). MR Imaging Characterization of Microvessels in Experimental Breast Tumors by Using a Particulate Contrast Agent with Histopathologic Correlation. *Radiology* 218: 562-569 [Abstract] [Full Text]

Radiology, Vol 207, 799-808, Copyright © 1998 by Radiological Society of North America

ARTICLES

Lymph node metastases: safety and effectiveness of MR imaging with ultrasmall superparamagnetic iron oxide particles--initial clinical experience

MF Bellin, C Roy, K Kinkel, D Thoumas, S Zaim, D Vanel, C Tuchmann, F Richard, D Jacqmin, A Delcourt, E Challier, T Lebret and P Cluzel
Department of Radiology, Hopital Pitie-Salpetriere, Paris, France.

PURPOSE: To evaluate the clinical and biologic safety of ultrasmall superparamagnetic iron oxide particles (AMI-227) as a contrast agent for magnetic resonance (MR) lymphography and to assess their efficacy for the differentiation of metastatic and benign nodes in patients with urologic and pelvic cancer. MATERIALS AND METHODS: Thirty adults suspected of having lymph node metastases underwent MR imaging before and 22-26 hours after intravenous infusion of AMI-227 (1.7 mg Fe/kg). Sixty histopathologically proved lymph nodes were analyzed on MR images, and 29 of these nodes were also analyzed quantitatively. RESULTS: AMI-227 was well tolerated with no major side effects. It allowed the detection of 10 additional nodes relative to those detected at MR imaging without AMI-227. None of the 27 metastatic nodes showed a decrease in signal intensity (SI) on AMI-227-enhanced images; nine of 27 metastatic nodes showed an increase in SI on T1-weighted images, probably resulting from altered capillary permeability in the tumor. A visually perceptible reduction in SI, indicating active AMI-227 uptake, was observed on postcontrast T2- and T2*-weighted images in 16 of 21 benign nodes. The SI ratio of benign nodes was lower than that of metastatic nodes on T2- and T2*-weighted images. The sensitivity of AMI- 227-enhanced MR lymphography was 100%, and the specificity was 80%. CONCLUSION: AMI-227 is safe and may facilitate the differentiation of metastatic and benign nodes in patients with urologic and pelvic cancers.

This article has been cited by other articles:

- Staatz, G., Nolte-Ernsting, C. C. A., Adam, G. B., Grosskortenhaus, S., Misselwitz, B., Bucker, A., Gunther, R. W. (2001). Interstitial T1-weighted MR Lymphography: Lipophilic Perfluorinated Gadolinium Chelates in Pigs. *Radiology* 220: 129-134 [Abstract] [Full Text]
- Hauger, O., Delalande, C., Deminière, C., Fouqueray, B., Ohayon, C., Garcia, S., Trillaud, H., Combe, C., Grenier, N. (2000). Nephrotoxic Nephritis and Obstructive Nephropathy: Evaluation

with MR Imaging Enhanced with **Ultrasmall Superparamagnetic Iron Oxide**-Preliminary Findings in a Rat Model. *Radiology* 217: 819-826 [Abstract] [Full Text]

- Sohaib, S. A. A., Richards, P. S., Ind, T., Jeyarajah, A. R., Shepherd, J. H., Jacobs, I. J., Reznek, R. H. (2002). MR Imaging of Carcinoma of the Vulva. *AJR* 178: 373-377 [Abstract] [Full Text]

(*Radiology*. 2000;217:819-826.)

Experimental Studies

Nephrotoxic Nephritis and Obstructive Nephropathy: Evaluation with MR Imaging Enhanced with Ultrasmall Superparamagnetic Iron Oxide-Preliminary Findings in a Rat Model[1]

Olivier Hauger, MD, Christophe Delalande, MS, Colette Deminière, MD, Bruno Fouqueray, MD, Céline Ohayon, PharmD, Stéphane Garcia, MD, Hervé Trillaud, MD, PhD, Christian Combe, MD, PhD and Nicolas Grenier, MD

[1] From the Unité Mixte de Recherche 5639, Centre National de la Recherche Scientifique (CNRS), Magnetic Resonance of Biologic Systems (O.H., C. Delalande, H.T., N.G.), and Hydrology and Environment Laboratory (C.O.), Université Victor Ségalen, 146 rue Léo Saignat, 33 076 Bordeaux, France; the Departments of Anatomic Pathology (C. Deminière) and Urology (S.G.), Hôpital Pellegrin, Bordeaux, France; the Unité Institut National de la Santé et de la Recherche Médicale (INSERM) U489, Paris, France (B.F.); and the Unité INSERM U441, Pessac, France (C.C.). Received September 17, 1999; revision requested November 2; revision received February 22, 2000; accepted February 23. Supported by the Société Française de Radiologie. **Address correspondence to** N.G. (e-mail: *nicolas.grenier@chu-bordeaux.fr*).

PURPOSE: To evaluate the role of magnetic resonance (MR) imaging enhanced with ultrasmall superparamagnetic iron oxide (USPIO) in the evaluation and differentiation of different types of nephropathies.

MATERIALS AND METHODS: Two experimental rat models of nephropathies were studied: a model of nephrotoxic nephritis induced by means of intravenous injection of sheep anti–rat glomerular basement membrane serum ($n = 43$) and a model of obstructive nephropathy ($n = 6$). Imaging sessions were performed with a spectrometer operating at 4.7 T with fast low-angle shot, or FLASH, sequences. Signal intensity was measured in each kidney compartment before and 24 hours after intravenous injection of USPIO (90 μmol of iron per kilogram of body weight). MR findings were compared with histologic data and urine protein levels.

RESULTS: In the nephrotoxic nephritis model 24 hours after injection of USPIO, a significant signal intensity decrease ($P < .05$) was present only in the cortex where the glomerular lesions were located. In the obstructive nephropathy model, the signal intensity decrease ($P < .05$) was located in all kidney compartments in response to diffuse interstitial lesions. The decrease in signal intensity was due to iron uptake by either macrophages or mesangial cells gaining endocytic activity and was correlated, in the

nephrotoxic nephritis model, to the degree of proteinuria.

CONCLUSION: Twenty-four-hour delayed USPIO-enhanced MR imaging may help identify and differentiate various types of nephropathies.

Index terms: Hydronephrosis, 81.84 • Iron • Kidney, MR, 81.121412, 81.12143 • Magnetic resonance (MR), contrast media, 81.12143 • Nephritis, 81.69

This article has been cited by other articles:

- PATRY, Y. C., TREWICK, D. C., GREGOIRE, M., AUDRAIN, M. A. P., MOREAU, A. M. N., MULLER, J.-Y., MEFLAH, K., ESNAULT, V. L. M. (2001). Rats Injected with Syngenic Rat Apoptotic Neutrophils Develop Antineutrophil Cytoplasmic Antibodies. *J Am Soc Nephrol* 12: 1764-1768 [Abstract] [Full Text]

DOI: 10.1148/radiol.2211001632
(*Radiology*. 2001;221:237-243.)

Experimental Studies

USPIO-enhanced Direct MR Imaging of Thrombus: Preclinical Evaluation in Rabbits[1]

Stephan A. Schmitz, MD, Sibylle Winterhalter, BA, Sascha Schiffler, BA, Robert Gust, BA, Susanne Wagner, DVM, Mayk Kresse, PhD, Sarah E. Coupland, MBBS, PhD, Wolfhard Semmler, MD, PhD and Karl-Jürgen Wolf, MD

[1] From the Department of Radiology and Nuclear Medicine (S.A.S., S. Winterhalter, S.S., R.G., K.J.W.) and the Department of Pathology (S.E.C.), Universitätsklinikum Benjamin Franklin, and the Institute of Diagnostic Research (M.K., W.S.), Freie Universität Berlin, Hindenburgdamm 30, 12200 Berlin, Germany; and the Department of Radiology, Charité, Humboldt Universität Berlin, Germany (S. Wagner). Received October 9, 2000; revision requested November 17; revision received May 2, 2001; accepted May 9. **Address correspondence to** S.A.S. (e-mail: *s.schmitz@medizin.fu-berlin.de*).

PURPOSE: To test the hypothesis that ultrasmall superparamagnetic iron oxide (USPIO) particles may diffuse into nonendothelialized fresh thrombi and thus allow for direct magnetic resonance (MR) imaging of a thrombus.

MATERIALS AND METHODS: Stagnation thrombi of different thrombus ages (1, 3, 5, 7, and 9 days) were induced in the external jugular veins of 25 rabbits. Direct MR imaging of thrombi was performed by using a fat-saturated T1-weighted gradient-echo sequence (three-dimensional [3D] magnetization prepared rapid acquisition gradient echo) before and 24 hours after intravenous administration of USPIO (particle size, 25 nm; 200 μmol per kilogram of body weight). Thrombus length on 3D reconstruction images was compared with that depicted on a radiographic venogram and with histologic findings (joint reference standard). In addition, T2*-weighted gradient-echo images were acquired and scored semiquantitatively.

RESULTS: The hyperintensity of the thrombus segment depicted on T1-weighted images (thrombus length determined with 3D reconstruction images divided by true thrombus length) increased significantly after administration of contrast medium at a thrombus age of 3 days (0.6 ± 0.4 [SD] to 0.8 ± 0.4; $P = .02$), 5 days (0.1 ± 0.1 to 1.0 ± 0.1; $P < .001$), and 7 days (0 to 0.6 ± 0.4; $P = .02$), but not at an age of 1 and 9 days. No significant change in the thrombus signal intensity was observed on T2*-weighted images.

CONCLUSION: The animal model showed that direct MR imaging of the thrombus improved 24 hours after USPIO administration with a T1-weighted sequence. No improvement was seen with the T2*-weighted sequence.

Index terms: Animals • Contrast media, experimental studies, 907.129412, 907.12943 • Contrast media, magnetic resonance (MR), 907.129412, 907.12943 • Embolism, experimental studies, 907.77 • Iron • Thrombosis, experimental studies, 907.751 • Thrombosis, MR, 907.751 • Veins, MR, 907.129412, 907.12943

(*Radiology*. 2001;218:562-569.)

Experimental Studies

MR Imaging Characterization of Microvessels in Experimental Breast Tumors by Using a Particulate Contrast Agent with Histopathologic Correlation[1]

Karl Turetschek, MD, Sabine Huber, MD, Eugenia Floyd, DVM, Thomas Helbich, MD, Timothy P. L. Roberts, PhD, David M. Shames, MD, Kirk S. Tarlo, PhD, Michael F. Wendland, PhD and Robert C. Brasch, MD

[1] From the Center for Pharmaceutical and Molecular Imaging, Department of Radiology, University of California, San Francisco, Box 0628, 505 Parnassus Ave, San Francisco, CA 94143-0628 (K.T., S.H., T.H., T.P.L.R., D.M.S., M.F.W., R.C.B.); Dept of Radiology, Univ of Vienna, Austria (K.T., T.H.); Dept of Radiology, KH Lainz, Vienna, Austria (S.H.); Dept of Pathology, Pfizer Central Research, Groton, Conn (E.F.); and Nycomed Amersham Imaging, Wayne, Pa (K.S.T.).
Received Feb 3, 2000; revision requested Mar 21; final revision received Jun 22; accepted Jun 28. Supported by NIH grant RO1 CA82923-01 and the Cancer Research Fund, State of Calif, interagency agreement #97-12013 with Dept of Health Services, Cancer Research Program. K.T. supported by a grant from the Max Kade Foundation. **Address correspondence to** R.C.B.

PURPOSE: To define the diagnostic potential of magnetic resonance (MR) imaging enhanced with ultrasmall superparamagnetic iron oxide (USPIO) particles for the quantitative characterization of tumor microvasculature.

MATERIALS AND METHODS: NC100150 injection, a USPIO in clinical trials, and albumin-(Gd-DTPA)$_{30}$ were compared at MR imaging on sequential days in the same 19 rats with mammary tumors. Kinetic analysis of dynamic T1-weighted three-dimensional spoiled gradient-recalled imaging data with a two-compartment bidirectional model yielded MR imaging estimates of microvascular permeability (K^{PS}) and fractional plasma volume (fPV) for each contrast medium.

RESULTS: Strongly positive and significant correlations were observed between MR imaging–derived K^{PS} estimates and histologic tumor grade with either the soluble albumin-(Gd-DTPA)$_{30}$ ($r = 0.88$; $P < .001$) or larger particulate USPIO ($r = 0.82$; $P < .001$). A significant correlation ($P < .05$) was observed with each contrast medium between K^{PS} and the histologic microvascular density (MVD), an angiogenesis indicator. Despite the considerable difference in molecule and particle sizes, no significant difference was observed in the MR imaging–derived mean permeability values generated with the two

contrast media.

CONCLUSION: USPIO, a macromolecular particulate MR imaging contrast agent, can be applied successfully to characterize tumor microvessels in animals. USPIO-derived K^{PS} correlated strongly with histopathologic tumor grade, MVD, and K^{PS} values derived by using albumin-$(Gd\text{-}DTPA)_{30}$ in the same tumors.

Index terms: Animals • Breast neoplasms, 00.30 • Contrast media • Iron • Magnetic resonance (MR), three-dimensional, 00.121411, 00.121412, 00.121419

Published online before print October 11, 2001, 10.1148/radiol.2213010220
(*Radiology*. 2001;221:822-826.)

Technical Developments

First-Pass Myocardial Perfusion MR Imaging with Outer-Volume Suppression and the Intravascular Contrast Agent NC100150 Injection: Preliminary Results in Eight Patients[1]

Tomas Bjerner, MD, Lars Johansson, Anders Ericsson, PhD, Gerhard Wikström, MD, PhD, Anders Hemmingsson, MD, PhD and Håkan Ahlström, MD, PhD

[1] From the Departments of Radiology (T.B., L.J., A.E., A.H., H.A.) and Cardiology (G.W.), University Hospital, S-751 85 Uppsala, Sweden; and Nycomed Amersham Imaging, Oslo, Norway (L.J.). Received January 3, 2001; revision requested February 14; revision received April 24; accepted May 21. Supported in part by Nycomed Amersham Imaging and Swedish Medical Research Council project 6676. **Address correspondence to** T.B. (e-mail: *Tomas.Bjerner@radiol.uu.se*).

The authors evaluated the feasibility of combining single-shot T2-weighted turbo spin-echo magnetic resonance (MR) imaging and first-pass myocardial perfusion MR imaging with an intravascular **ultrasmall superparamagnetic iron oxide** (USPIO) contrast agent, NC100150 Injection (3 mg of iron per kilogram of body weight). Eight patients with coronary vessel disease underwent T2-weighted turbo spin-echo MR imaging (in-plane resolution, 1–2 mm) during the first pass of the USPIO contrast agent. The mean decrease in signal intensity in myocardium perfused by a nonstenotic coronary artery was 59% ± 13 (SD) ($P < .012$) This method is feasible for imaging of myocardial perfusion.

Index terms: Heart, perfusion, 511.12144 • Magnetic resonance (MR), contrast enhancement, 511.12143 • Myocardium, blood supply, 511.76, 511.771 • Myocardium, MR, 511.121412

BC

IEEE TRANSACTIONS ON MAGNETICS, VOL. 24, NO. 2, MARCH 1988

PROTEINS AND CARBOHYDRATES AS ALTERNATIVE SURFACTANTS FOR THE PREPARATION OF STABLE MAGNETIC FLUIDS

A. Wooding, M. Kilner and D.B. Lambrick

Department of Chemistry, Durham University, South Road, Durham, DH1 3LE.

ABSTRACT

A one-stage preparation of stable aqueous magnetic fluids is reported, whereby colloidal Fe_3O_4 particles are dispersed using naturally occurring polymers and their derivatives (e.g. gelatine, poly-galacturonic acid, carboxymethyl-cellulose and succinylated gelatine) as surfactant materials. Low toxicity materials have been used to permit possible medical use of the fluids. Through using a variety of surfactant concentrations at the time of particle formation, control of particle size has been achieved, and particles as small as 3.0 nm diameter obtained. Stable fluids with up to 6% Fe_3O_4 content can be produced, having magnetisations of ca. 2 $JT^{-1}Kg^{-1}$ (20 Gauss). Fluids diluted 30 fold remain stable colloids.

INTRODUCTION

Ferrofluids containing magnetite may be prepared using a variety of techniques, the two most important being ball-milling [1] and precipitation from aqueous solution. [2] In the ball milling process, powdered magnetite with particles sizes in the micron range is milled in the presence of a carrier liquid and surfactant, often for weeks until the particles are of colloidal size. Though the method is time consuming and produces a wide distribution of particle sizes, typically 2-50 nm, never-the-less it is extremely versatile, producing fluids with almost any carrier liquid and surfactant [1,3]. The main alternative method involves the addition of base to an aqueous mixture of iron(II) and iron(III) in a 1:2 molar ratio. The surfactant is then added to the colloidal particles in a separate stage, prior to separation of the particles, usually having a narrow size distribution from the aqueous solution and re-dispersion in other carrier/surfactant mixtures [2]. More recently, stable aqueous ferrofluids have been prepared without the use of a surfactant, by the peptization of magnetite particles in both alkaline and acid media with consequent charge stabilization. Low polarizability of the counterion is an essential consideration in the correct choice of acid or base [4].

We report the formation of water-based magnetic fluids containing up to 6% magnetite by base treatment of mixed iron(II) and iron(III) solutions containing naturally occurring polymeric dispersing agents, and their derivatives. A range of proteins and polysaccharides appear to be suitable for this purpose, and typical compounds reported here are gelatine, poly-galacturonic acid, carboxymethylcellulose, and succinylated gelatine. The expected low toxicity of the resultant fluids gives them potential for medical applications, including use as drug carriers or drug anchors (e.g. cancer treatment) and for other targeting and mapping purposes.

Control of the size and size distribution of the resulting magnetic particles has been achieved by careful monitoring of the amount of dispersing agent used in the preparation. Particles as small as 3 nm, and with a narrow size distribution, have been prepared in this way, and provide two desirable features for application purposes. Firstly, fluid stability toward gravitational and magnetic forces is enhanced by the small size, and secondly, the large surface area of the magnetite per unit mass provides a large potential for the attachment of other materials, such as drugs.

EXPERIMENTAL

Iron(II) and iron(III) chlorides, sodium hydroxide and succinic anhydride were general purpose chemicals which were used without further purification. Gelatine, poly-galacturonic acid (PGA), and carboxymethylcellulose (CMC) were obtained as analytical grade products from Sigma Chemical Company and were also used without further purification.

Succinylated gelatine was prepared [5] by adding succinic anhydride (15 g) in small aliquots, to a solution of gelatine (15 g) in H_2O (600 ml) at room temperature over a period of 1 hour, maintaining a pH of 7-10 by occasional additions of concentrated sodium hydroxide solution. The succinylated gelatine solution was passed through a column of Amberlite IRA 400 anion exchange resin to remove excess succinate ions. Excess water was then removed under vacuum at 50°C to obtain the desired concentration using a rotary evaporator.

i) Fluid preparation:

To a solution of iron(II) chloride tetrahydrate (0.85 gms) in deaerated water (10 ml) was added a polymeric surfactant solution (x gms in 60 ml H_2O, where x varies between 0.5 and 8) and the mixture heated to 80°C with stirring under a steady flow of nitrogen. 33% aqueous ammonia (2 ml) was then added to precipitate iron(II) hydroxide. Meanwhile a suspension of iron(III) hydroxide was prepared by adding 33% aqueous ammonia (12 ml) to ferric chloride (2.33 gms) dissolved in 20 ml deaerated water (20 ml) at 80°C.

The iron(III) hydroxide suspension at 80°C was now added to the suspension of iron(II) hydroxide surfactant mixture at 80°C with stirring to precipitate the black magnetic oxide. After 5 mins. at 80°C the suspension was cooled to room temperature. Portions were removed and agitated for 10 mins. by means of an ultrasonic probe. This disperses the particle agglomerates and produces a stable magnetic fluid. Using the above quantities 1 gm Fe_3O_4 was produced. In cases where the surfactant : Fe_3O_4 mass-ratio $\leq$ 2:1, additional surfactant must be added immediately after Fe_3O_4 formation to ensure complete dispersal. An anionic surfactant, "Sarkosyl-'o'" is suitable for this purpose.

RESULTS

Particle sizes and size distributions were estimated using the following techniques.

i) Electron Microscopy:

Transmission electron micrographs (TEM) were taken at magnifications between 220,000 and 360,000 and analysed

0018-9464/88/0300-1650$01.00©1988 IEEE

using an automated image analyser, interfaced to a computer [6]. A typical micrograph of a well dispersed gelatin ferrofluid is shown in Figure 1 below.

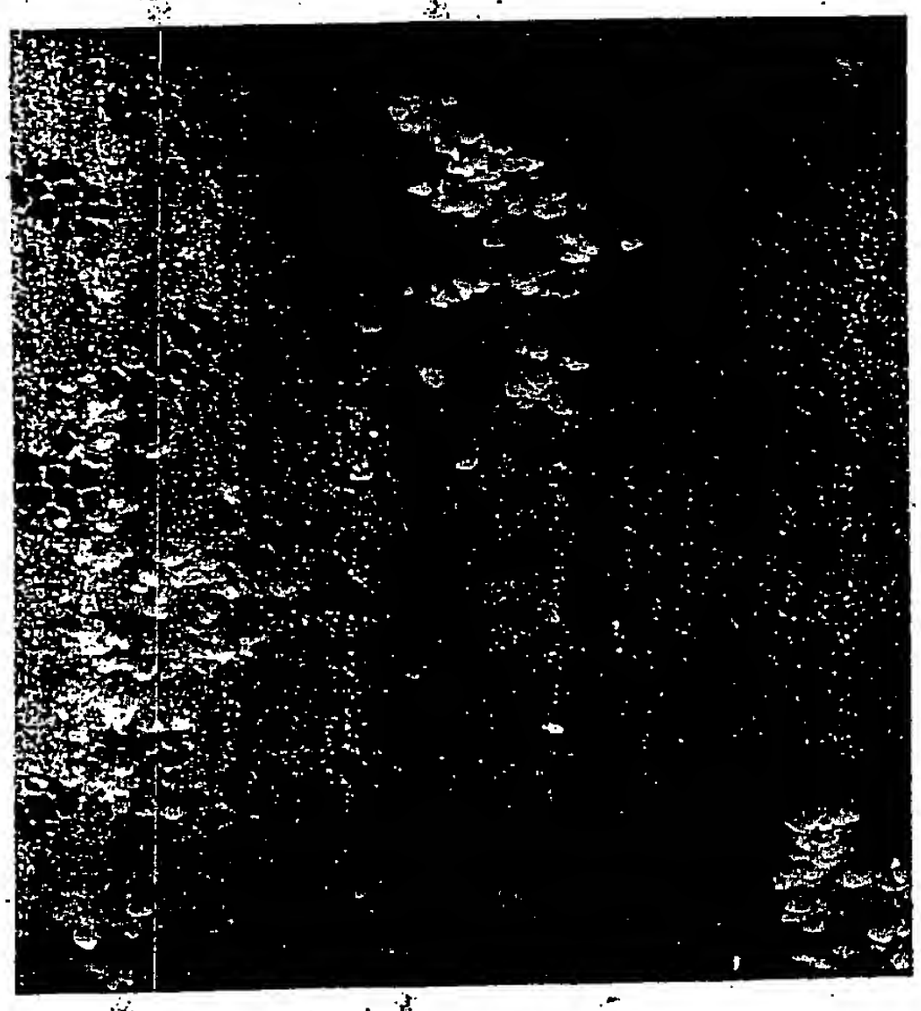

Figure 1. A typical gelatin ferrofluid as viewed at 280,000 magnification

Mean sizes (D_v) and size distributions (σ) obtained from such photographs are displayed in computer-generated histogram form in Figure 2, for a set of fluids each containing a different quantity of gelatin present at the time of preparation.

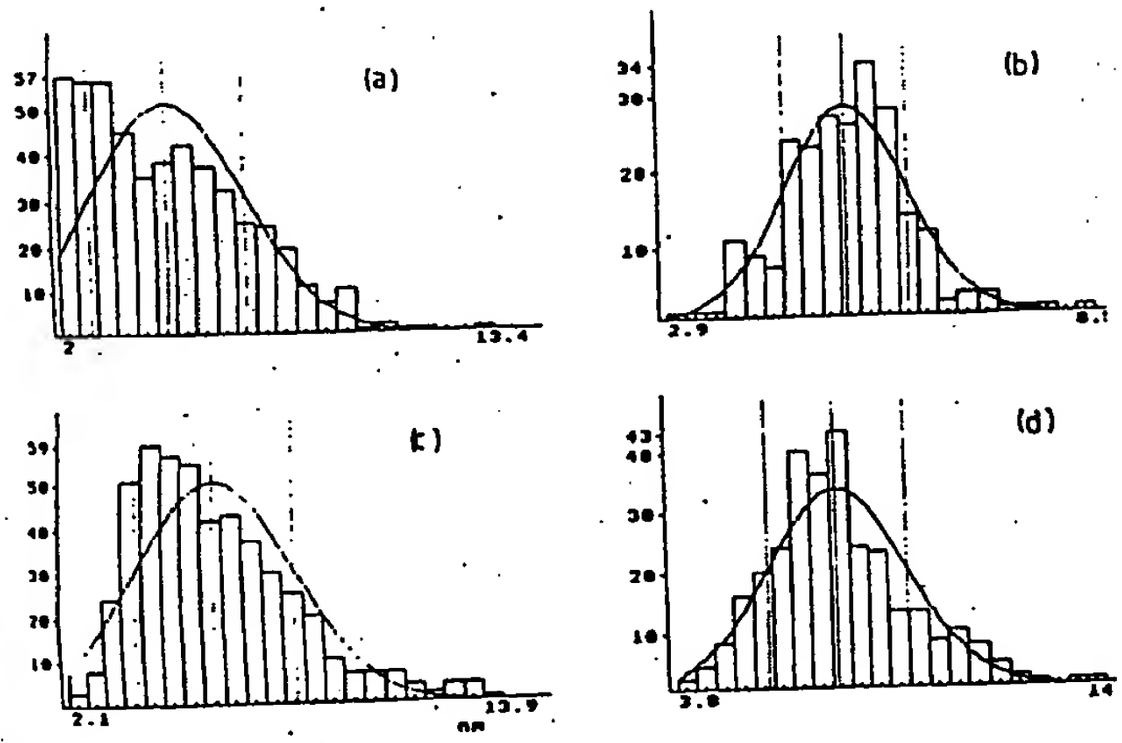

Figure 2. Diameter distributions of fluids containing a) 8 gms, b) 5 gms, c) 2 gms, d) 1 gm gelatine

ii) Magnetic Analysis:

Magnetization curves were obtained for each fluid using a Vibrating Sample Magnetometer and were corrected for both diamagnetic (sample holder) and demagnetizing effects (spherical samples were used). Saturation magnetizations obtained for the gelatine systems were of the order of 2 $JT^{-1}Kg^{-1}$, which corresponds to a 6% weighting of magnetic material in the fluid. Values of ~ 4% were obtained when PGA or CMC was substituted for gelatine.

The method of Chantrell [7] has been applied to obtain magnetic particle diameters (D_v) and the corresponding standard deviations (σ). This data, along with that obtained from TEM, are presented in Table 1 for all fluids prepared.

ANALYSIS OF RESULTS AND DISCUSSION

The formation of soluble complexes of gelatine and transition metal ions (in particular Fe^{2+} and Fe^{3+}) above pH 5 is well documented [8,9]. The process is believed to occur via proton loss from the side chain carboxyl groups (i.e. glutamic or aspartic amino-acid residues) along the polymer chain and subsequent complexation with the metal ion. This ionization is almost complete at pH 5 whereas iron(II) hydroxide does not begin to form before pH 6-7. Hence a situation may be envisaged whereby, as the pH of a gelatine/iron(II) chloride solution is increased from pH 2 upwards, the gelatine/iron(II) complexes will form before iron(II) hydroxide. This is likely to have two effects.

TABLE 1
Size Data for Polymer Stabilised Magnetic Fluids

Surfactant	Mass Ratio, Surfactant:Fe_3O_4 Used in Preparation	TEM (Å) D_v	TEM (Å) σ	Magnetic Chantrell (Å) D_v	Magnetic Chantrell (Å) σ
Gelatin	8	57.8	21.1	62.4	22
Gelatin	5	52.4	8.7	51.3	15.7
Gelatin	3.5	57.4	13	45.9	18.9
Gelatin	2	61.2	22.1	46.7	27.3
Gelatin	1	76	17.5	49.6	23.3
Gelatin	0.5	79.2	23	46.4	24.4
SG	5	61.1	20	44	22
SG	2	44.9	13.4	42	16.4
SG	1	71.1	18.2	53.6	21.2
PGA	8	30.1	7.8	40.7	13.0
PGA	5	35.3	8.2	49.2	14.3
PGA	2	37.7	10.8	44	18.5
PGA	1	45.4	12.7	52.3	19.7
PGA	0.5	54.9	14.2	59.2	20.2
CMC	4	49.6	15	61.2	19.6
CMC	2	40.2	10.1	52.5	20
CMC	1	46.8	14.5	50.5	20.2
No Surfactant	No Surfactant	61	22.1	60.9	25.4

i) It creates the maximum amount of nucleation sites since iron(II) hydroxide forms whilst iron(II) ions are coordinated individually to sites on the gelatine, prior to formation of a mixed valent oxide.

ii) Formation of particles of a fairly uniform size, i.e. 5.2 nm using a gelatine:Fe_3O_4 ratio of 5:1. Interestingly this ratio corresponds to one gelatine carboxyl group for each iron(II) ion. These groups on gelatine are regularly spaced about 10 amino-acid residues of 5 nm apart [10], and since the particles are also 5 nm in diameter, this may imply uniform crystal growth at each carboxyl coordination site along the gelatine backbone. It is conceivable that growth will continue until it is sterically hindered by other particles growing in the same region of the gelatine. Thus particle size control here may be a direct consequence of the chemical and structural features of the protein used.

The TEM data would appear to support the above theory. As the above ratio of 5:1 is decreased, thereby reducing the number of available carboxyl groups for coordination, the average particle size increases, and most noticeably, the standard deviation.

rises significantly (Table 1 and Figures 2c,2d). These features may be interpreted in terms of insufficient nucleation sites on the gelatine present, to maintain growth only on gelatine coordinated particles. Some magnetite therefore forms independently of the gelatine chain, and subsequent crystal growth is consequently unimpaired. Larger particles are found in such samples. It is relevant to note that as the amount of gelatine is successively reduced, the average particle size increases, giving credance to this possible explanation.

When the system contains a large proportion of gelatine, creating a large excess of carboxyl groups over iron(II) species, then according to the above model, both small and large particles should grow along the polymer chain, particle size being governed by to what extent they are allowed to grow before encountering another particle. It is found experimentally that at a ratio of 8:1 gelatine:magnetite, 5.8 nm particles with a wide size distribution (see also Fig. 2a) are formed.

To test whether the size changes could arise from changes in viscosity of aqueous gelatine solutions, parallel experiments using polyethylene glycol a non surface-active viscosity increasing agent [11], were undertaken. Such experiments have eliminated changes in viscosity as being responsible for the above particle size effects.

The number of potential coordination sites on the gelatine may be increased by treating gelatine with succinic anhydride, which attaches succinyl groups to the side chain amino-groups [5]. Use of succinylated gelatine in the magnetic preparation was expected, on the basis of the previous model, to lead to smaller particle sizes than gelatine alone. Indeed at an optimum ratio of 2:1 (SG:Fe_3O_4), smaller particles (4.5 nm), having a narrow size distribution, were obtained compared with the use of the parent gelatine. Again ratios either side of this ideal concentration gave increases in particle size and standard deviation.

The magnetic particle sizes for gelatin and succinylated gelatin based fluids are consistently smaller than their TEM counterparts and do not appear to reflect the same trends. Lack of agreement is more pronounced at low surfactant concentrations. These differences serve to illustrate the following effects:

i) Even at low surfactant concentrations viscosity within the reaction medium is significant. This will suppress the rate of molecular collisions between iron(II) and iron(III) species and hence particle formation. Oxidation of iron(II) hydroxide in the interim period upsets the stoichiometric ratio of iron(II) and iron(III) required for Fe_3O_4 formation. The excess of iron(III) shows up as non-ferromagnetic 'dead layers' on the surface of particles [12], undetected by magnetic analysis but included in TEM size determinations.

ii) The method of Chantrell [7] tends to overlook very small particles because of the large applied fields required to align their magnetic moments. Mean sizes obtained by magnetic analysis for samples containing very small particles will thus be exaggerated.

The first effect will predominate in gelatin based fluids where sizes are typically 50-80 Å, whilst the latter effect takes over in PGA and CMC based fluids where 30-50 Å particles are observed physically.

PGA and CMC are both linear polysaccharides with at least one carboxyl group per glycoside unit. This places such groups no more than 10 Å apart [13] and as such, magnetic particles of a similar dimension might be expected. However, particles no smaller than 30 Å have been observed. The extensive hydrogen bonding which exists between polymer chains at high surfactant concentrations may serve to block carboxyl groups from complexing with iron(II) ions and would, according to the previous model, explain the absence of sub-30 Å particles.

Comparing the data for these two systems with that for gelatine reveals the same trends of increasing size and standard deviation as the polymer concentration decreases from the optimum value.

The magnetic fluids remain stable colloids on dilution, and 30 fold dilution has been achieved without separation of magnetic material.

CONCLUSIONS

The preparation of very small magnetite particles with narrow size distributions has been achieved using proteins and carbohydrates, whilst control of particle size has been achieved by varying the concentration of dispersing agent. The reproducible fluids thus prepared were stable colloids in both gravitational and magnetic fields. Since the proteins and carbohydrates used are potentially non toxic, the fluids described offer advantages over micron sized magnetic particles currently finding applications in medicine.

REFERENCES

1. S.S. Papell, U.S. Patent, 3,215,572, (1965).
2. G.W. Reimers and S.E. Khalafalla, U.S. Patent 3,843,540, (1970).
3. R.E. Rosensweig and R. Kaiser, NTIS Rep. No. NASW-1219, NASA Rep. NASA-CRa91684. NASA Office of Adv. Res. and Tech., Washington D.C., (1967).
4. R. Massart, IEEE Trans. Magn., Vol. MAG-17, No. 2, 1247-48 (1981)
5. G.E. Heans and R.E. Feeney, "Chemical Modifications of Proteins", (1971), Holden-Day. Inc., San Francisco.
6. S.R. Hoon , D.B. Lambrick and D.H. Paige, J. Phys. E. Sci. Instrum., 18, 389, (1985).
7. R.W. Chantrell, J. Popplewell and S.W. Charles, IEEE Trans. Magn. MAG-14, 975, (1978).
8. J. Bello and J.R. Vinograd, Nature, 181, 273, (1958).
9. R.H.H. Wolf and K. Ester, J. Col. Polym. Sci., 252, 570, (1974).
10. J.E. Eastoe and J.E. Leach, Sci. Technol. Gelatin. 73-107, (1977), Academic Press, New York, A.G. Ward and A. Court (Edts.).
11. J.P.S. Arora et al, Tenside Detergents, 21, 87 (1984)
12. C.P. Bean and J.D. Livingston, J. Appl. Phys., 30, 1205, (1959).
13. E.A. MacGregor and C.T. Greenwood, "Polymers in Nature", 1980, Wiley and Sons, Toronto.